Monomeric (Pentamethylcyclopentadienyl)iridium Imido Compounds: Synthesis, Structure, and Reactivity

David S. Glueck, Jianxin Wu, Frederick J. Hollander, and Robert G. Bergman*

Contribution from the Department of Chemistry, University of California, Berkeley, California 94720. *Received August 20, 1990*

Abstract: The monomeric terminal imido complexes Cp*IrNR (Cp* = η^5-C_5Me_5; **1a**, R = *t*-Bu; **1b**, R = $SiMe_2t$-Bu; **1c**, R = 2,6-$Me_2C_6H_3$; **1d**, R = 2,6-*i*-$Pr_2C_6H_3$) were prepared from $[Cp^*IrCl_2]_2$ (**2**) and 4 equiv of the corresponding lithium amide LiNHR in THF. In addition, the complexes $Cp^*Ir(RNH_2)Cl_2$ (**3a**, R = *t*-Bu; **3d**, R = 2,6-*i*-$Pr_2C_6H_3$) were made from an amine and $[Cp^*IrCl_2]_2$ (**2**) and dehydrochlorinated with $KN(SiMe_3)_2$ to provide an alternate route to **1a,d**. Efficient exchange occurred between **1a** and arylamines, leading to **1c,d** and *tert*-butylamine. *tert*-Butylimido complex **1a**, a weak nucleophile, reacted with MeI to form $[Cp^*IrI_2]_2$ and Me_3Nt-Bu^+I^-. Coupling of the imido ligand in **1a** with CN*t*-Bu and CO gave $Cp^*Ir(t$-BuNCN*t*-Bu)(CN*t*-Bu) (**4**) and $Cp^*Ir(t$-BuNCO)(CO) (**5a**), respectively. $Cp^*IrPPh_3(t$-BuNCO) (**5b**) was formed from **1a**, PPh_3, and CO. The bridging imido complex Cp*IrN*t*-Bu(dppePt) (**6**, dppe = 1,2-bis(diphenylphosphino)ethane) was prepared from **1a** and dppePt(C_2H_4). Complex **1a** and CO_2 gave the cycloadduct $Cp^*Ir(N$*t*-BuOCO) (**7a**), which added PPh_3 to form $Cp^*IrPPh_3(N$*t*-BuOCO) (**7b**). Two equivalents of dimethylacetylenedicarboxylate reacted with **1a** to yield the pyrrole complex Cp(Ir(η^4-RCCRN*t*-BuRCCR) (**8**, R = CO_2Me). Maleic anhydride was added to **1a** to give $Cp^*Ir[N$*t*-BuC(O)CH=$CHCO_2$] (**9a**), which reacted with CO to yield $Cp^*Ir(CO)[N$*t*-BuC(O)CH=$CHCO_2$] (**9b**). Compounds **1a–d**, **7a**, and **8** were structurally characterized by X-ray diffraction; imido complexes **1a–d** have short Ir–N distances and nearly linear Ir–N–C(Si) angles, consistent with the presence of a metal–nitrogen triple bond.

Introduction

Many oxo (M=O) and imido (M=NR) complexes of metals in the middle (V–Mn triads) of the transition series are known.[1] These compounds are often unreactive, despite the suggestion that imido species are involved in the Haber ammonia synthesis, nitrile reduction, and the ammoxidation of propylene.[2] The reactivity of OsO_4 and related imido compounds[3] and the recent preparation of reactive zirconium–imido complexes[4] suggests that moving away from the middle of the periodic table may change the properties of the metal–ligand multiple bond in these compounds and improve the chances of utilizing them in oxo- and imido-transfer reactions. This paper reports a simple conversion of $[Cp^*IrCl_2]_2$ to the imido complexes Cp*IrNR (R = *t*-Bu, $SiMe_2t$-Bu, 2,6-$Me_2C_6H_3$, 2,6-*i*-$Pr_2C_6H_3$). Surprisingly, these compounds are monomeric, but as expected they exhibit novel reactivity, including transfer of the NR group to electrophilic substrates.

Results

Synthesis and Spectroscopic Characterization of the Iridium Imido Compounds Cp*IrNR. Treatment of $[Cp^*IrCl_2]_2$ (**2**)[5] with 4 equiv of LiNHR in tetrahydrofuran gives the compounds Cp*IrNR as yellow-to-orange crystals in high yield [Scheme I: **1a**, R = *t*-Bu; **1b**, R = $SiMe_2t$-Bu; **1c**, R = Xy (2,6-$Me_2C_6H_3$); **1d**, R = DIPP (2,6-*i*-$Pr_2C_6H_3$)]. These reactions can be run on a gram scale, and the products are easily recrystallized from cold pentane. The amine RNH_2 is a byproduct; gas chromatography showed that *tert*-butylamine was formed in 56% yield (integration vs a cyclohexane standard) along with **1a**. Unlike the isoelectronic oxo complex $[Cp^*IrO]_2$,[6] the new imido compounds are not highly sensitive to air or moisture, but they gradually turn brown over a period of days even as solids under nitrogen, presumably due to slow thermal decomposition.

Scheme I

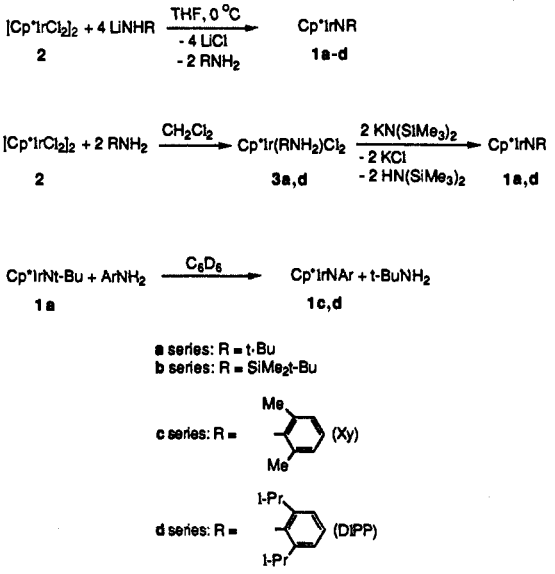

Dehydrohalogenation of the amine complexes $Cp^*Ir(RNH_2)Cl_2$ (**3a**, R = *t*-Bu; **3d**, R = DIPP) with $KN(SiMe_3)_2$, as shown in Scheme I, provides a related route to compounds **1a** and **1d**. This method, however, gives lower yields. Compounds **3a,d** are easily prepared by cleavage of the dimer $[Cp^*IrCl_2]_2$ (**2**) with primary amines; they form air-stable crystals with physical properties similar to those of the well-known phosphine compounds $Cp^*IrPR_3Cl_2$. The IR spectra of **3a,d** contain two NH stretches, and the NH protons were also observed in the ^1H NMR spectra.

A third synthetic route to arylimide complexes involves treatment of *tert*-butylimido compound **1a** with arylamines to give **1c,d** and *tert*-butylamine (Scheme I). When **1a** is treated with

(1) (a) For leading references, see: (a) Nugent, W. A.; Mayer, J. M. *Metal–Ligand Multiple Bonds*; Wiley-Interscience: New York, 1988. (b) Nugent, W. A.; Haymore, B. L. *Coord. Chem. Rev.* **1980**, *31*, 123. For leading references to imido-containing clusters, see ref 15g and references therein. A portion of the results described here has been reported in preliminary form: (c) Glueck, D. S.; Hollander, F. J.; Bergman, R. G. *J. Am. Chem. Soc.* **1989**, *111*, 2719. Tables of positional and thermal parameters for **1a** and **7a** were included as supplementary material for this communication.

(2) (a) Nugent, W. A. *Inorg. Chem.* **1983**, *22*, 965 and references therein. (b) Chan, D. M.-T.; Fultz, W. C.; Nugent, W. A.; Roe, D. C.; Tulip, T. H. *J. Am. Chem. Soc.* **1985**, *107*, 251.

(3) (a) Reference 1a, pp 252–255. (b) For some examples of reactive osmium–imido compounds, see: Chong, A. O.; Oshima, K.; Sharpless, K. B. *J. Am. Chem. Soc.* **1977**, *99*, 3420.

(4) (a) Walsh, P. J.; Hollander, F. J.; Bergman, R. G. *J. Am. Chem. Soc.* **1988**, *110*, 8729. (b) Cummins, C. C.; Baxter, S. M.; Wolczanski, P. T. *J. Am. Chem. Soc.* **1988**, *110*, 8731.

(5) Ball, R. G.; Graham, W. A. G.; Heinekey, D. M.; Hoyano, J. K.; McMaster, A. D.; Mattson, B. M.; Michel, S. T. *Inorg. Chem.* **1990**, *29*, 2023.

(6) (a) McGhee, W. D.; Foo, T.; Hollander, F. J.; Bergman, R. G. *J. Am. Chem. Soc.* **1988**, *110*, 8543. (b) McGhee, W. D. Ph.D. Thesis, UC Berkeley, 1987.

0002-7863/91/1513-2041$02.50/0

Table I. Crystal and Data Collection Parameters[a]

	1a	1b	1c	1d	7a	8
temp (°C)	25	25	−100	−85	25	25
empirical formula	$IrNC_{14}H_{24}$	$IrSiNC_{16}H_{30}$	$IrNC_{18}H_{24}$	$IrNC_{22}H_{32}$	$IrO_2NC_{15}H_{24}$	$IrO_8NC_{26}H_{36}$
formula weight (amu)	398.6	456.7	446.6	502.7	442.6	682.8
crystal size (mm)	0.25 × 0.37 × 0.42	0.20 × 0.30 × 0.33	0.15 × 0.22 × 0.30	0.25 × 0.30 × 0.45	0.05 × 0.20 × 0.55	0.25 × 0.25 × 0.25
space group	*Pbcm*	$P2_1/m$	$I4_1/a$	*Pnma*	*Pnma*	$P2_1/n$
a(Å)	9.3284 (16)	7.4892 (10)	28.521 (5)	13.798 (3)	17.7036 (22)	9.6892 (12)
b(Å)	13.2916 (19)	12.2481 (23)	28.521 (5)	17.230 (3)	11.4994 (11)	17.7125 (17)
c(Å)	12.3250 (19)	10.7990 (13)	8.2367 (15)	8.753 (1)	7.8632 (6)	16.4649 (18)
α(deg)	90.0	90.0	90.0	90.0	90.0	90.0
β(deg)	90.0	106.455 (10)	90.0	90.0	90.0	100.999 (8)
γ(deg)	90.0	90.0	90.0	90.0	90.0	90.0
V(Å^3)	1528.2 (7)	950.0 (4)	6700.2 (35)	2081.1 (10)	1600.8 (4)	2773.8 (10)
Z	4	2	16	4	4	4
d_{calc} (g cm^{-3})	1.73	1.60	1.77	1.60	1.84	1.63
μ_{calc} (cm^{-1})	86.8	70.5	79.3	63.9	83.1	48.4
reflctns measd	$+h,+k,\pm l$	$+h,+k,\pm l$	$+h,+k,+l$	$+h,+k,+l$	$+h,-k,+l$	$+h,+k,\pm l$
scan width	$\Delta\theta$ = 0.65 + 0.35 tan θ	$\Delta\theta$ = 0.60 + 0.35 tan θ	$\Delta\theta$ = 0.70 + 0.35 tan θ	$\Delta\theta$ = 0.65 + 0.35 tan θ	$\Delta\theta$ = 0.60 + 0.35 tan θ	$\Delta\theta$ = 0.55 + 0.35 tan θ
scan speed (θ, deg/m)	0.78→6.70	0.72→6.70	6.70	6.70	1.08→6.70	0.66→6.70
setting angles (2θ, deg)[b]	28–30	28–32	24–28	26–28	28–30	28–30

[a] Parameters common to all structures: radiation, Mo Kα (λ = 0.71073 Å); monochromator, highly oriented graphite (2θ = 12.2°); detector, crystal scintillation counter, with PHA; 2θ range, 3→45°, except for **1c** 2→45°; scan type, θ–2θ; background, measured over 0.25($\Delta\theta$) added to each end of the scan; vertical aperture = 3.0 mm; horizontal aperture = 2.0 + 1.0 tan θ mm; intensity standards, measured every hour of x-ray exposure time; orientation, three reflections were checked after every 200 measurements. Crystal orientation was redetermined if any of the reflections were offset from their predicted positions by more than 0.1°. Reorientation was required twice for **1b** and **7a** and once for **8**. [b] Unit cell parameters and their esd's were derived by a least-squares fit to the setting angles of the unresolved Mo Kα components of 24 reflections with the given 2θ range. In this and all subsequent tables the esd's of all parameters are given in parentheses, right-justified to the least significant digit(s) of the reported value.

1 equiv or an excess of xylylamine, *tert*-butylamine and **1c** are formed within 1 day. Under these conditions, however, **1c** slowly decomposes to an unidentified purple material which contains a 1:1 ratio of Cp* and xylyl groups according to its ^{1}H NMR spectrum. Isolated Cp*IrNXy decomposes to this same material when treated with xylylamine. Cp*IrNDIPP (**1d**) is formed slowly along with *tert*-butylamine from **1a** and $DIPPNH_2$; in this case the half-life of the reaction is about 2 days, and the product is stable to the reaction conditions.

Imido compound **1a** was identified spectroscopically. In the ^{1}H NMR spectrum, the signal due to the *tert*-butyl methyl protons appears as a triplet (J = 1.6 Hz) as a result of coupling to ^{14}N (I = 1). This coupling is characteristic of compounds having axially symmetric electron density at the nitrogen nucleus, as has been observed previously in other imido complexes and in alkyl isonitriles, and suggested a linear M–N–C linkage.[7a] The labeled analogue Cp*Ir^{15}N*t*-Bu ([^{15}N]-**1a**) was prepared from $[Cp^*IrCl_2]_2$ and Li^{15}N*H*t-Bu as described in the Experimental Section. In its ^{1}H NMR spectrum, the *t*-Bu signal appears as a doublet (J = 2.4 Hz) with coupling to ^{15}N ($I = {}^1/_2$).[7b] The complex exhibited a broadened singlet in the ^{15}N NMR spectrum at δ −71.8 ppm relative to CH_3NO_2 external standard (C_6D_6 solvent). Complex **1a** also displays an intense IR absorption at 1258 cm^{-1}, characteristic of the imido ligand. As in other IR studies of imido complexes, the assignment of this band to a M≡N or a C—N vibration is difficult. A simple harmonic oscillator model for the Ir≡N stretch predicts a shift to 1218 cm^{-1} on ^{15}N substitution, but in [^{15}N]-**1a** this band moves to 1240 cm^{-1}, as predicted for the C—N stretch. The observed absorption, however, may be due to a combination of the M≡N and C—N stretches, not a diatomic oscillator.[8] The electron impact (EI) mass spectrum of **1a** shows molecular ions at m/e 399 and 397 for the two iridium-containing isotopomers.

For the other imido complexes **1b–d**, no ^{14}N–^{1}H coupling was observed in the ^{1}H NMR spectrum, presumably because of changes in ^{14}N and ^{1}H relaxation rates, which may be associated with the reduced symmetry at nitrogen. These compounds were identified by NMR, IR, and mass spectroscopy. Silylimido compound **1b** displayed an IR spectrum similar to that of **1a**, with an intense peak at 1117 cm^{-1}. The arylimides **1c,d**, however, show several strong bands in the IR spectra. Like **1a**, **1b** and **1d** gave molecular ions in the EI mass spectra. For **1c**, however, the EI mass spectrum showed a parent ion at m/e 894/892, the correct mass for a dimer. A similar misleading result was observed in the fast atom bombardment (FAB) mass spectrum for **1a**, presumably due to ion–molecule reactions in the mass spectrometer.

Structures of the Imido Complexes. The structures of **1a–d** were determined by X-ray crystallography. The structures were solved by Patterson methods and refined via standard least-squares and Fourier techniques. Crystal and data collection parameters are shown in Table I, and details of the diffraction studies are given in the Experimental Section. ORTEP diagrams for **1a–d** are shown in Figure 1. Table IIa–d contains bond lengths and angles for these compounds.

A single yellow, blocky crystal of **1a** was obtained by crystallization from pentane at −40 °C. The structure confirms that **1a** is a monomer, as suggested by the ^{1}H NMR and mass spectra. The complex adopts a "one-legged piano stool" or "pogo-stick" geometry. The Ir–N–C angle (177.2 (5)°) is nearly linear, and the Ir–N bond length (1.712 (7) Å) is very short. The silylimido compound **1b**, crystallized from pentane at −40 °C, has a similar structure with an Ir–N bond length of 1.750 (3) Å and an Ir–N–Si angle of 170.8 (2)°. The arylimido compounds Cp*IrNAr (**1c**, Ar = Xy; **1d**, Ar = DIPP) are very similar with bond lengths and angles intermediate between **1a** and **1b** (for **1c**, Ir–N = 1.729 (7) Å and the Ir–N–C angle is 174.9 (7)°, and for **1d**, Ir–N = 1.749 (7) Å and the Ir–N–C angle is 174.0 (6)°). Table III compares selected metrical data for **1a–d**.

Reactivity of Cp*IrN*t*-Bu (1a). In addition to its exchange reactions with arylamines (Scheme I), Cp*IrN*t*-Bu (**1a**) undergoes several reactions with small molecules in which the imido ligand acts as a weak base or nucleophile. For example, it reacts with an excess of methyl iodide to form the known $[Cp^*IrI_2]_2$[9] and $[Me_3N$*t*-Bu$]^+I^-$ (eq 1). The ammonium salt was identified by comparison of its ^{1}H NMR and IR spectra to those of an authentic

(7) (a) See ref 1b, p 143, and references therein. For a more recent example, see: Fjare, D. E., Gladfelter, W. L. *J. Am. Chem. Soc.* **1981**, *103*, 1572. (b) The observed coupling constants are consistent with the formula $J(^{14}N–X) = -0.713\ J(^{15}N–X)$ derived from the magnetogyric ratios of the N isotopes. Gordon, A. J.; Ford, R. A. *The Chemist's Companion*; Wiley-Interscience: New York, 1971; p 299.

(8) See ref 1a, pp 123–125, and references therein.

(9) (a) Booth, B. L.; Haszeldine, R. N.; Hill, M. *J. Organomet. Chem.* **1969**, *16*, 491. (b) Gill, D. S.; Maitlis, P. M. *J. Organomet. Chem.* **1975**, *87*, 359.

Table II. Intramolecular Bond Distances and Angles for **1a–d**

atom 1	atom 2	distance	atom 1	atom 2	atom 3	angle	atom 1	atom 2	distance	atom 1	atom 2	atom 3	angle
						a. Compound **1a**							
Ir	C4	2.177 (7)	Cp	Ir	N	179.2							
Ir	C5	2.194 (5)	Ir	N	C1	177.2 (5)				C4	C5	C6	107.4 (5)
Ir	C6	2.205 (5)					C4	C5	1.415 (6)	C5	C6	C6	108.1 (3)
Ir	CP	1.832	N	C1	C2	108.2 (5)	C4	C7	1.520 (10)	C5	C4	C7	125.3 (3)
Ir	N	1.712 (7)	N	C1	C3	108.9 (6)	C5	C6	1.422 (6)	C4	C5	C8	125.9 (4)
			C2	C1	C2	105.0 (10)	C5	C8	1.491 (8)	C6	C5	C8	126.6 (5)
N	C1	1.447 (11)	C2	C1	C3	113.2 (6)	C6	C6	1.424 (13)	C5	C6	C9	126.0 (6)
C1	C2	1.480 (10)					C6	C9	1.494 (6)	C6	C6	C9	125.8 (3)
C1	C3	1.429 (11)	C5	C4	C5	109.2 (5)							
						b. Compound **1b**							
Ir	N	1.750 (3)	Cp	Ir	N	177.29				C3	C2	C4	108.7 (3)
Ir	C5	2.170 (4)	Ir	N	Si	170.8 (2)				C4	C2	C4	110.7 (5)
Ir	C6	2.191 (3)					C5	C6	1.420 (4)	C6	C5	C6	108.4 (4)
Ir	C7	2.204 (3)					C5	C8	1.509 (7)	C6	C5	C8	125.8 (2)
Ir	CP	1.830					C6	C7	1.418 (4)	C5	C6	C7	107.6 (3)
N	SI	1.715 (3)	N	Si	C1	108.95 (14)	C6	C9	1.500 (5)	C5	C6	C9	125.2 (3)
Si	C1	1.858 (4)	N	Si	C2	107.9 (2)	C7	C7	1.416 (7)	C7	C6	C9	127.1 (3)
Si	C2	1.884 (5)	C1	Si	C1	108.1 (3)	C7	C10	1.496 (5)	C6	C7	C7	108.2 (2)
C2	C3	1.551 (7)	C1	Si	C2	111.47 (16)				C6	C7	C10	125.8 (3)
C2	C4	1.536 (6)	SI	C2	C3	109.4 (4)				C7	C7	C10	126.0 (2)
			S1	C2	C4	109.6 (3)							
						c. Compound **1c**							
Ir	N	1.729 (7)	Cp	Ir	N	176.7	C16	C18	1.497 (14)	C2	C1	C5	107.5 (8)
Ir	C1	2.206 (9)	Ir	N	C11	174.9 (7)				C1	C2	C3	109.5 (8)
Ir	C2	2.159 (9)					C1	C2	1.436 (13)	C2	C3	C4	106.9 (8)
Ir	C3	2.179 (9)	N	C11	C12	119.3 (8)	C1	C5	1.418 (12)	C3	C4	C5	106.6 (8)
Ir	C4	2.190 (9)	N	C11	C16	119.6 (9)	C2	C3	1.430 (13)	C1	C5	C4	109.6 (8)
Ir	C5	2.201 (9)	C12	C11	C16	121.1 (9)	C3	C4	1.473 (13)	C2	C1	C6	125.6 (8)
Ir	CP	1.812	C11	C12	C13	118.8 (9)	C4	C5	1.443 (13)	C5	C1	C6	126.9 (9)
			C11	C12	C17	120.5 (9)	C1	C6	1.514 (13)	C1	C2	C7	125.3 (8)
N	C11	1.379 (11)	C13	C12	C17	120.6 (10)	C2	C7	1.502 (13)	C3	C2	C7	125.1 (9)
C11	C12	1.396 (13)	C12	C13	C14	118.6 (11)	C3	C8	1.470 (14)	C2	C3	C8	126.9 (9)
C11	C16	1.436 (13)	C13	C14	C15	123.8 (11)	C4	C9	1.484 (13)	C4	C3	C8	126.2 (9)
C12	C13	1.429 (14)	C14	C15	C16	119.5 (10)	C5	C10	1.513 (13)	C3	C4	C9	125.5 (9)
C13	C14	1.384 (15)	C11	C16	C15	117.9 (9)				C5	C4	C9	127.6 (8)
C14	C15	1.351 (14)	C11	C16	C18	120.5 (9)				C1	C5	C10	127.2 (9)
C15	C16	1.426 (14)	C15	C16	C18	121.4 (10)				C4	C5	C10	123.2 (8)
C12	C17	1.494 (14)											
						d. Compound **1d**							
Ir	N	1.749 (7)	Cp	Ir	N	177.80	C3	C4	1.387 (8)	C2	C5	C7	113.9 (5)
Ir	C8	2.167 (9)	Ir	N	C1	174.0 (6)	C5	C6	1.554 (8)	C6	C5	C7	108.7 (5)
Ir	C9	2.179 (6)	N	C1	C2	119.4 (4)	C5	C7	1.544 (9)	C9	C8	C9	109.2 (7)
Ir	C10	2.198 (6)	C2	C1	C2	121.2 (7)	C8	C9	1.405 (7)	C9	C8	C11	125.4 (4)
Ir	CP	1.816	C1	C2	C3	118.5 (5)	C8	C11	1.516 (12)	C8	C9	C10	108.0 (5)
			C1	C2	C5	118.2 (5)	C9	C10	1.445 (8)	C8	C9	C12	126.2 (5)
N	C1	1.352 (9)	C3	C2	C5	123.3 (5)	C9	C12	1.517 (9)	C10	C9	C12	125.7 (5)
C1	C2	1.414 (7)	C2	C3	C4	120.3 (6)	C10	C10	1.428 (11)	C9	C10	C10	107.4 (3)
C2	C3	1.410 (8)	C3	C4	C3	121.3 (9)	C10	C13	1.504 (8)	C9	C10	C13	126.7 (5)
C2	C5	1.535 (8)	C2	C5	C6	109.4 (5)				C10	C10	C13	125.9 (3)

Table III. Selected Bond Lengths (Å) and Angles (deg) for the Imido Compounds Cp*IrNR (**1a–d**)

	R =			
	R = *t*-Bu	$SiMe_2t$-Bu	R = Xy	R = DIPP
Ir–N	1.712 (7)	1.750 (3)	1.729 (7)	1.749 (7)
N–C(Si)	1.447 (11)	1.715 (3)	1.379 (11)	1.352 (9)
∠Ir–N–C(Si)	177.2 (5)	170.8 (2)	174.9 (7)	174.0 (6)

sample prepared by repeated methylation (with MeI) and deprotonation of LiNH*t*-Bu.

$$Cp^*IrNt\text{-}Bu + xs\ MeI \longrightarrow [Cp^*IrI_2]_2 + Me_3Nt\text{-}Bu^+I^- \quad (1)$$

1a

Complex **1a** reacts with 2 equiv of *tert*-butyl isocyanide to form $Cp^*Ir(CNt\text{-}Bu)(C(Nt\text{-}Bu)_2)$ (**4**) in which one isocyanide has added across the Ir–N multiple bond to form a carbodiimide, and the resulting 16-electron complex has been trapped by another isocyanide (Scheme II). Addition of 1 equiv of isocyanide affords a 1:1 mixture of **1a** and **4**. The structure of complex **4** was suggested by its IR spectrum [ν_{CN} = 2065 cm^{-1} with a shoulder

Scheme II

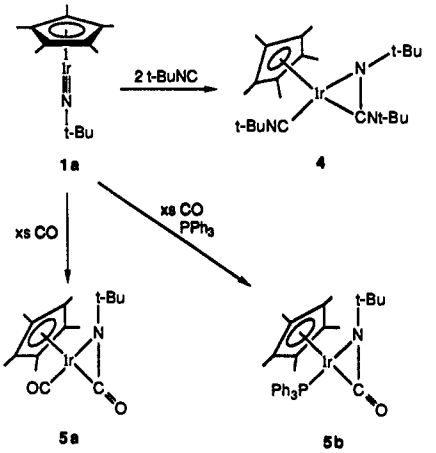

at 2110 cm^{-1} (terminal isocyanide) and ν_{CN} = 1688 cm^{-1} with a shoulder at 1707 cm^{-1} (carbodiimide)]. The ^{13}C NMR spectrum

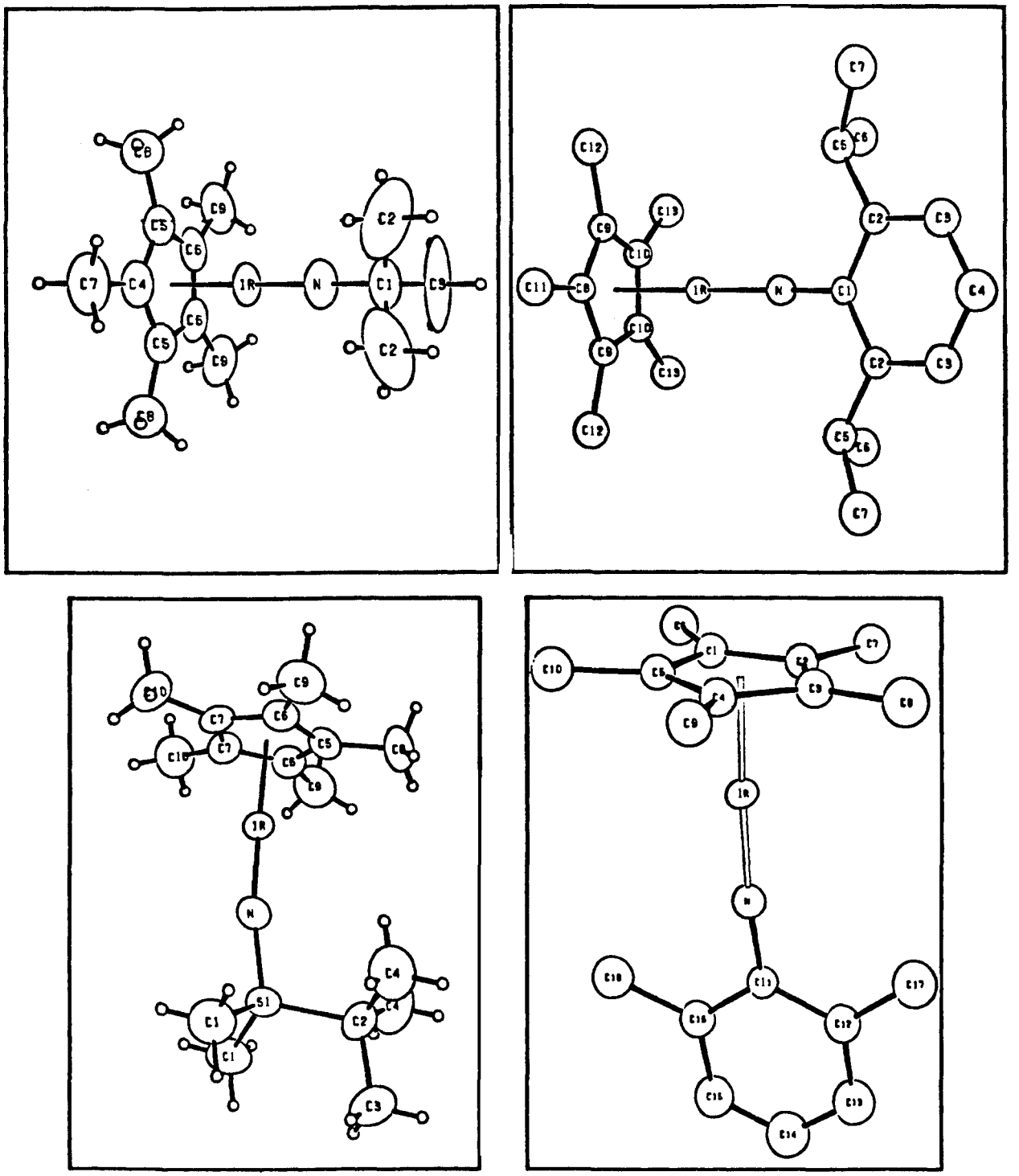

Figure 1. ORTEP drawings of **1a–d**, counterclockwise from the upper left-hand corner.

shows signals due to the isocyanide and carbodiimide carbons at δ 138.6 and 137.8.

As shown in Scheme II, compound **1a** undergoes a similar coupling–trapping reaction with an excess of CO to form the carbonyl *tert*-butyl isocyanate complex Cp*Ir(CO)(*t*-BuNCO) (**5a**) [ν_{CO} = 1956 and 1801 cm^{-1}, ^{13}C NMR δ 174.7 and 143.5]. When CO is added to a mixture of **1a** and PPh_3 (1 equiv), the phosphine *tert*-butyl isocyanate complex Cp*IrPPh$_3$(*t*-BuNCO) (**5b**) can be isolated in good yield, and the carbonyl compound Cp*Ir(CO)(*t*-BuNCO) (**5a**) is not observed. The new triphenylphosphine compound shows an isocyanate CO stretch at 1751 cm^{-1} in the IR spectrum, and the *tert*-butyl isocyanate carbon appears at δ 140.7 in the ^{13}C NMR spectrum with the expected coupling to phosphorus (J_{P-C} = 7.2 Hz). Compound **5a** is stable under a CO atmosphere, but **5b** is slowly converted to Cp*IrPPh$_3$(CO)[10] and *t*-BuNCO according to ^{31}P and ^{1}H NMR spectroscopy.

Air-stable orange dppePt(Cp*IrN*t*-Bu) (**6**, dppe = 1,2-bis(diphenylphosphino)ethane) and ethylene are formed from complex **1a** and dppePt(C_2H_4) (eq 2). The bridging imido compound **6** was identified by NMR spectroscopy. As in the isoelectronic alkyne complexes dppePt(RCCR′),[11] the ^{31}P NMR spectrum contains two doublets (J_{P-P} = 55.6 Hz) with ^{195}Pt satellites (J_{Pt-P} = 3991 and 2663 Hz). The P–P coupling is characteristic of dppe bound to Pt(0), and the Pt–P couplings suggest that the metal–imido moiety is not bound symmetrically to the Pt center. The

(10) Glueck, D. S.; Newman, L. J.; Bergman, R. G., submitted for publication.

(11) Simpson, R. D.; Bergman, R. G., unpublished results.

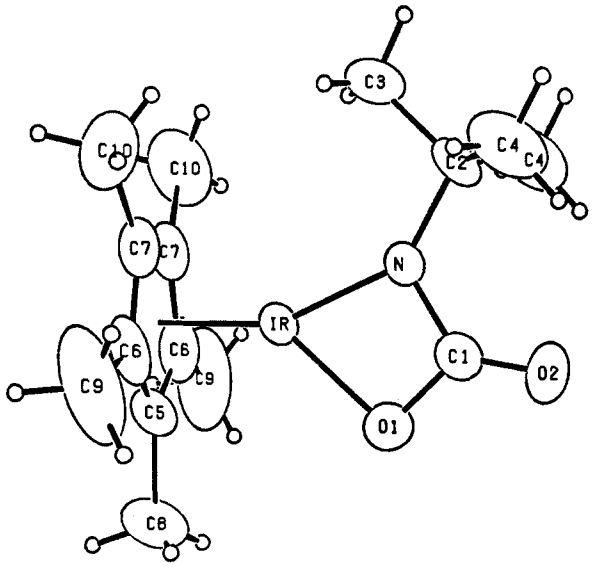

Figure 2. ORTEP drawing of **7a**.

Scheme III

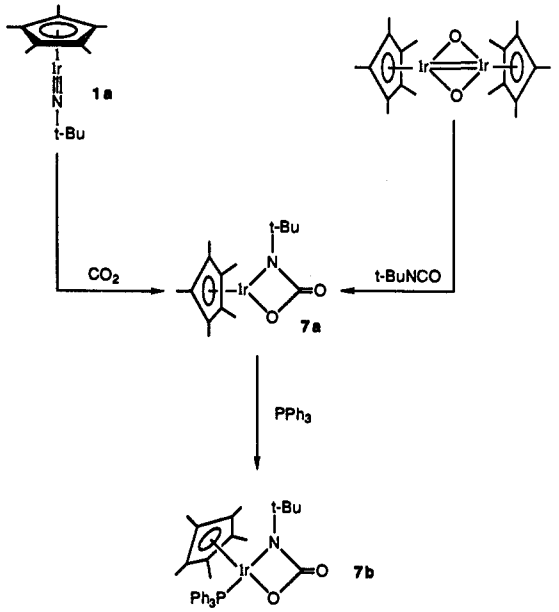

$NCMe_3$ carbon shifts from δ 59.0 in free **1a** to δ 70.0 and shows coupling to phosphorus, as expected.

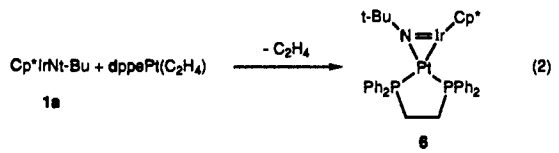

Complex **1a** reacts with carbon dioxide to yield red crystals of the cycloadduct Cp*Ir(N*t*-BuOCO) (**7a**). This material exhibits spectral properties consistent with the structure illustrated in Scheme III [IR ν_{CO} = 1708 cm^{-1}; ^{13}C NMR δ 170.9 for the CO_2 carbon; MS molecular ion at *m/e* 443/441]. Crystals of **7a** suitable for X-ray analysis were obtained by vapor diffusion of hexamethyldisiloxane into toluene at −40 °C. The structure was solved by Patterson methods and refined by standard least-squares and Fourier techniques. Details are given in the Experimental Section and in Table I. An ORTEP diagram of the four-membered metallacycle is shown in Figure 2; bond lengths and angles are given in Table IV. In comparison to **1a**, the Ir–N bond has lengthened (to 1.943 (6) Å), and the Ir–N–C angle has decreased (to 141.6 (5)°) upon cycloaddition with CO_2. The N–C bond length increases slightly (from 1.447 (11) to 1.488 (9) Å). Complex **7a** has also been prepared in these laboratories by the addition of *t*-BuNCO to $[Cp^*IrO]_2$.[12]

Table IV. Intramolecular Bond Distances and Angles for **7a**

atom 1	atom 2	distance	atom 1	atom 2	atom 3	angle
Ir	O1	2.049 (6)	O1	Ir	N	65.35 (22)
Ir	N	1.943 (6)	O1	Ir	Cp	139.60
Ir	C5	2.159 (8)	N	Ir	Cp	155.05
Ir	C6	2.137 (5)				
Ir	C7	2.157 (5)	Ir	O1	C1	93.7 (4)
Ir	CP	1.780	O1	C1	O2	124.7 (7)
			O1	C1	N	105.1 (6)
C1	O1	1.320 (9)	O2	C1	N	130.3 (7)
C1	O2	1.191 (9)	Ir	N	C1	95.9 (4)
C1	N	1.397 (9)	Ir	N	C2	141.6 (5)
N	C2	1.488 (9)	C1	N	C2	122.5 (6)
C2	C3	1.515 (12)	N	C2	C3	107.5 (6)
C2	C4	1.518 (7)	N	C2	C4	108.9 (4)
			C3	C2	C4	110.4 (5)
C5	C6	1.414 (8)	C4	C2	C4	110.7 (7)
C5	C8	1.491 (14)				
C6	C7	1.431 (8)	C6	C5	C6	107.2 (7)
C6	C9	1.504 (8)	C6	C5	C8	126.4 (4)
C7	C7	1.380 (10)	C5	C6	C7	108.2 (5)
C7	C10	1.530 (8)	C5	C6	C9	127.0 (7)
			C7	C6	C9	124.8 (7)
			C6	C7	C7	108.2 (3)
			C6	C7	C10	124.3 (6)
			C7	C7	C10	127.3 (4)

Coordinatively unsaturated **7a** reacts rapidly with PPh_3 to give the yellow 18-electron adduct Cp*IrPPh$_3$(N*t*-BuOCO) (**7b**). Compound **7b** was identified by IR (ν_{CO} = 1621 cm^{-1}) and ^{13}C NMR (δ 166.5 for the CO_2 carbon). This compound is exceptionally moisture-sensitive and reacts with traces of water to form *tert*-butylamine and what we presume is the carbonate complex Cp*IrPPh$_3$(CO_3), whose PMe_3 analogue is known.[13]

Complex **1a** also adds 2 equiv of dimethylacetylenedicarboxylate to form the substituted pyrrole complex **8** (eq 3). The stoichiometry of this reaction was determined by integration of the carboxylate methyl signals in the ^1H NMR spectrum and confirmed by elemental analysis and mass spectrometry. Addition of 1 equiv of the alkyne yields a 1:1 mixture of product and starting material. The ^1H NMR spectrum of **8** from 20 to −70 °C shows two signals for the carboxylate methyl protons in addition to signals due to the Cp* and *tert*-butyl protons. The ^{13}C NMR spectrum contains signals due to the pairs of inequivalent carbonyl, carboxylate, and acetylenic carbons. The IR spectrum shows a strong peak at 1723 cm^{-1} with a shoulder at 1703 cm^{-1}

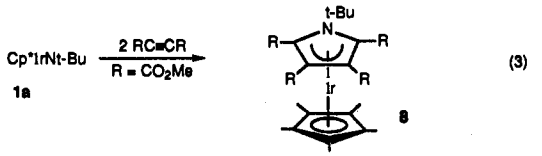

A single-crystal X-ray diffraction study was performed on a yellow platelike crystal of **8** obtained from diffusion of hexamethyldisiloxane into a toluene solution of the compound at −40 °C. The structure was solved by Patterson methods and refined by standard least-squares and Fourier techniques. Details are given in the Experimental Section and in Table I. The ORTEP diagram (Figure 3) shows that a substituted pyrrole has been formed from the two alkynes and the N*t*-Bu ligand; it acts as an η^4 ligand to the Ir center. The Ir–N distance of 2.74 Å is out of bonding range, and the N*t*-Bu group is bent away from the Ir (the dihedral angle between the plane of the four bound ring carbons C_{11}–C_{14} and the plane formed by C_{11}–N–C_{14} is 37.0 (0.3)°). Bond lengths

(12) McGhee, W. D.; Bergman, R. G., unpublished results.
(13) Sponsler, M. B.; Bergman, R. G., unpublished results.

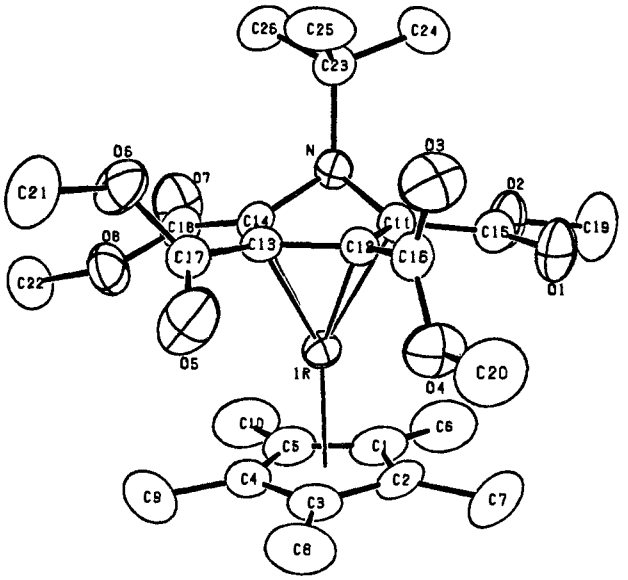

Figure 3. ORTEP drawing of **8**.

Scheme IV

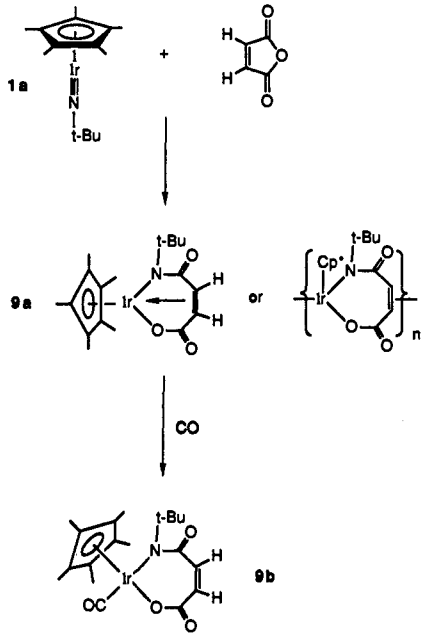

and angles are given in Table V.

The η^4-pyrrole is not bound to Ir as a simple diene. C_{12} and C_{13} are slightly closer to the Ir than N-bound C_{11} and C_{14}. The C–N bonds (1.459 (4) and 1.469 (4) Å) are typical of C–N single bonds. The C–C bonds in the pyrrole are significantly shorter than C–C single bonds but longer than usually encountered for delocalized double bonds. The C_{12}–C_{13} distance of 1.436 (5) Å is similar to the average C–C bond length in the Cp* ligand of this compound (1.426 Å), but the other two bonds (1.460 (5) Å for C_{11}–C_{12} and 1.480 (5) Å for C_{13}–C_{14}) are significantly longer.

Maleic anhydride reacts with **1a** to give a compound that elemental analysis and mass spectrometry show is a 1:1 adduct of the imido complex and the olefin. The ^{1}H NMR spectrum of this adduct is essentially invariant from −63 °C to 70 °C, at which point decomposition becomes rapid. It displays signals due to inequivalent C–H protons at δ 5.33 and 4.90 (acetone-d_6) which are coupled to one another (J = 9.8 Hz). The CH protons in free maleic anhydride resonate at δ 7.29 (acetone-d_6). This observation and the correspondingly large coordination chemical shift of the CH carbons (from δ 137.5 in free maleic anhydride to δ 83.3 and 83.0 in the complex) suggest that the olefinic carbons are coordinated in a π fashion to the Ir. The ^{13}C NMR spectrum also contains peaks due to two inequivalent carbonyl groups.

We suggest that this adduct has one of the structures shown as **9a** (Scheme IV). In an apparently similar process, reaction of $Cp^*IrPPh_3(OEt)(H)$ with maleic anhydride gives $Cp^*IrPPh_3(O_2CCH{=}CHCO_2Et)(H)$ as a result of nucleophilic attack of ethoxide at the anhydride carbonyl and ring-opening with coordination of the anhydride oxygen to Ir.[10] In analogy to this, we suggest that **9a** is formed by nucleophilic attack of

Table V. Intramolecular Bond Distances and Angles for **8**

atom 1	atom 2	distance	atom 1	atom 2	atom 3	angle
Ir	C1	2.200 (4)	Cp	Ir	C11	144.85 (10)
Ir	C2	2.211 (4)	Cp	Ir	C12	148.30 (9)
Ir	C3	2.245 (4)	Cp	Ir	C13	149.04 (9)
Ir	C4	2.211 (4)	Cp	Ir	C14	145.24 (9)
Ir	C5	2.212 (4)	C11	Ir	C12	40.48 (12)
Ir	C11	2.132 (3)	C11	Ir	C13	64.98 (13)
Ir	C12	2.087 (3)	C11	Ir	C14	59.72 (13)
Ir	C13	2.106 (3)	C12	Ir	C13	40.05 (12)
Ir	C14	2.152 (3)	C12	Ir	C14	65.52 (13)
Ir	CP	1.854 (1)	C13	Ir	C14	40.65 (14)
			C11	N	C14	93.5 (2)
N	C11	1.459 (4)	N	C11	C12	111.8 (3)
N	C14	1.469 (4)	C11	C12	C13	103.6 (3)
C11	C12	1.460 (5)	C12	C13	C14	103.8 (3)
C12	C13	1.436 (5)	C13	C14	N	110.3 (3)
C13	C14	1.480 (5)	Ir	C11	C15	115.3 (3)
C11	C15	1.476 (5)	N	C11	C15	124.7 (3)
C12	C16	1.508 (5)	C12	C11	C15	121.2 (3)
C13	C17	1.482 (5)	Ir	C12	C16	129.1 (3)
C14	C18	1.458 (5)	C11	C12	C16	129.4 (3)
C15	O1	1.196 (5)	C13	C12	C16	126.2 (3)
C15	O2	1.338 (5)	Ir	C13	C17	126.4 (2)
C16	O3	1.198 (4)	C12	C13	C17	123.7 (3)
C16	O4	1.304 (5)	C14	C13	C17	132.4 (3)
C17	O5	1.196 (4)	Ir	C14	C18	114.4 (2)
C17	O6	1.315 (5)	N	C14	C18	121.4 (3)
C18	O7	1.190 (4)	C13	C14	C18	126.9 (3)
C18	O8	1.358 (5)	O1	C15	O2	123.8 (4)
O2	C19	1.450 (5)	O1	C15	C11	124.4 (4)
O4	C20	1.451 (5)	O2	C15	C11	111.8 (3)
O6	C21	1.447 (5)	O3	C16	O4	125.9 (3)
O8	C22	1.449 (4)	O3	C16	C12	121.2 (4)
N	C23	1.519 (5)	O4	C16	C12	112.9 (3)
C23	C24	1.524 (5)	O5	C17	O6	123.5 (3)
C23	C25	1.531 (5)	O5	C17	C13	124.6 (3)
C23	C26	1.523 (6)	O6	C17	C13	111.8 (3)
			O7	C18	O8	123.0 (3)
			O7	C18	C14	126.6 (4)
			O8	C18	C14	110.3 (3)
			C15	O2	C19	115.9 (3)
C1	C2	1.445 (6)	C16	O4	C20	116.6 (3)
C1	C5	1.401 (6)	C17	O6	C21	116.1 (3)
C1	C6	1.488 (6)	C18	O8	C22	115.8 (3)
C2	C3	1.434 (6)	C11	N	C23	116.3 (3)
C2	C7	1.498 (6)	C14	N	C23	117.0 (3)
C3	C4	1.425 (5)	N	C23	C24	107.6 (3)
C3	C8	1.493 (6)	N	C23	C25	114.7 (3)
C4	C5	1.426 (6)	N	C23	C26	107.7 (3)
C4	C9	1.511 (6)	C24	C23	C25	108.6 (3)
C5	C10	1.503 (6)	C24	C23	C26	109.1 (3)
			C25	C23	C26	109.1 (4)
			C2	C1	C5	108.4 (4)
			C2	C1	C6	124.5 (4)
			C5	C1	C6	126.9 (4)
			C1	C2	C3	107.3 (4)
			C1	C2	C7	126.5 (4)
			C3	C2	C7	125.9 (4)
			C2	C3	C4	107.4 (4)
			C2	C3	C8	126.4 (4)
			C4	C3	C8	126.3 (4)
			C3	C4	C5	108.6 (4)
			C3	C4	C9	124.6 (4)
			C5	C4	C9	126.4 (4)
			C1	C5	C4	108.2 (3)
			C1	C5	C10	126.6 (4)
			C4	C5	C10	125.1 (4)

Table VI. ^{1}H NMR Data[a]

compound	δ (ppm)	mult	J (Hz)	assignment	integral
1a, Cp*IrN*t*-Bu	2.07			C_5Me_5	15
	1.32	t	1.6	*t-Bu*	9
1b, Cp*IrNSiMe$_2$*t*-Bu	1.95			C_5Me_5	15
	1.11			*t-Bu*	9
	0.17			$SiMe_2$	6
1c, Cp*IrNXy	7.0	t	7	*p*-C_6H_3	1
	6.9	d	7	*m*-C_6H_3	2
	2.39			*o-Me*	6
	1.99			C_5Me_5	15
1d, Cp*IrNDIPP	7.21	t	7.7	Ph	1
	6.98	d	7.7	Ph	2
	4.06	sept	6.9	C*H*Me$_2$	2
	1.98			C_5Me_5	15
	1.35	d	7.0	CH*Me*$_2$	12
3a, Cp*Ir(*t*-BuNH$_2$)Cl$_2$[d]	3.65	br		NH_2	2
	1.61			C_5Me_5	15
	1.29			*t*-Bu	9
3d, Cp*Ir(DIPPNH$_2$)Cl$_2$[d]	7.14	m		Ph	3
	5.64	br		NH_2	2
	3.24	sept	6.7	C*H*Me$_2$	2
	1.30			C_5Me_5	15
	1.28	d	6	CH*Me*$_2$	12
4. Cp*Ir(CN*t*-Bu)(*t*-BuNCN*t*-Bu)	1.80			C_5Me_5	15
	1.67			*t-Bu*	9
	1.38			*t-Bu*	9
	1.07			*t-Bu*	9
5a, Cp*Ir(CO)(*t*-BuNCO)	1.64			C_5Me_5	15
	1.12			*t-Bu*	9
5b, Cp*IrPPh$_3$(*t*-BuNCO)	7.80–7.74	m		P*Ph*$_3$	6
	7.10–7.00	m		P*Ph*$_3$	9
	1.62	d	1.2	C_5Me_5	15
	0.95			*t-Bu*	9
6, Cp*IrN*t*-Bu(dppe Pt)[c]	8.21–8.15	m		*o-Ph*	4
	7.60–7.55	m		*o-Ph*	4
	7.38–7.36	m		*m,p-Ph*	6
	7.25	m		*m,p-Ph*	6
	2.04–1.92	m		P*CH*$_2$	4
	1.74			C_5Me_5	15
	1.21			*t-Bu*	9
7a, Cp*Ir(N*t*-BuOCO)	1.52			C_5Me_5	15
	1.22			*t-Bu*	9
7b, Cp*IrPPh$_3$(N*t*-BuOCO)	7.7–7.6	m		P*Ph*$_3$	6
	7.1–7.0	m		P*Ph*$_3$	9
	1.32			*t-Bu*	9
	1.20	d	2.0	C_5Me_5	15
8, Cp*Ir-(RCCRN*t*-BuRCCR)[b] (R = CO_2Me)	3.52			CO_2Me	6
	3.46			CO_2Me	6
	1.67			C_5Me_5	15
	1.21			*t-Bu*	9
9a, Cp*Ir-[N*t*-BuC(O)CH=CHCO$_2$]	5.33	d	9.8	C*H*	1
	4.90	d	9.9	C*H*	1
	1.92			C_5Me_5	15
	1.27			*t-Bu*	9
9b, Cp*Ir(CO)-[N*t*-BuC(O)CH=CHCO$_2$]	7.32	d	6.5	C*H*	1
	7.20	d	6.5	C*H*	1
	1.72			*t-Bu*	9
	1.31			C_5Me_5	15

[a] All spectra in C_6D_6 at 20 °C unless indicated. [b] Acetone-d_6. [c] THF-d_8. [d] CD_2Cl_2.

N*t*-Bu on the anhydride carbonyl, followed by coordination of the anhydride oxygen to the metal. The structures shown in Scheme IV are consistent with the spectroscopic observations and account for coordination of the olefinic carbons to the metal as well. A monomeric structure for **9a** appears unlikely due to the strain in the seven-membered ring required for Ir–olefin coordination; this and the limited solubility of the compound suggest that the alternative oligomeric structure shown in Scheme IV is correct.

Compound **9a** can be carbonylated in acetone solution at 45 °C to give **9b**, Cp*Ir(CO)(N*t*-BuC(O)CH=CHCO$_2$), formed by displacement of the olefinic linkage from Ir by carbon monoxide. The CO ligand produces an IR stretch at 1994 cm^{-1} and a resonance in the ^{13}C spectrum at δ 184.2. The olefinic carbons are no longer coordinated to the Ir center (^{1}H NMR δ 7.32 and 7.20 (doublets, with J = 6.5 Hz); ^{13}C {^{1}H} NMR δ 141.0 and 137.3, similar to the chemical shifts of the free alkene). Unlike **9a**, monomeric complex **9b** is freely soluble in benzene.

Discussion

Preparation of New Iridium Imido Compounds. Compounds **1a–d** are the first fully characterized monomeric terminal imido compounds to be prepared by using metals lying to the right of the Fe triad in the periodic table. Previously Stone and co-workers prepared several complexes with fluorinated alkyl–imido groups,[14] and some compounds with bridging imido ligands are known.[15]

(14) For monomeric terminal imido compounds of the late (groups 9–11) transition metals, see: (a) Ashley-Smith, J.; Green, M.; Mayne, N.; Stone, F. G. A. *J. Chem. Soc., Chem. Commun.* **1969**, 409. (b) McGlinchey, M. J.; Stone, F. G. A. *J. Chem. Soc., Chem. Commun.* **1970**, 12655. (c) Ashley-Smith, J.; Green, M.; Stone, F. G. A. *J. Chem. Soc., Dalton Trans.* **1972**, 1805.

Table VII. $^{13}C\{^1H\}$ NMR Data[a]

compound	δ (ppm)	mult	J (Hz)	assignment
1a, Cp*IrN*t*-Bu	84.8			C_5Me_5
	59.0			CMe_3
	29.6			CMe_3
	11.7			C_5Me_5
1b, Cp*IrNSiMe$_2$*t*-Bu	86.2			C_5Me_5
	26.4			CMe_3
	18.8			CMe_3
	11.4			C_5Me_5
	−3.7			$SiMe_2$
1c, Cp*IrNXy	150.2			N–*C*
	133.3			*Ph*
	127.3			*Ph*
	122.8			*Ph*
	85.9			C_5Me_5
	18.6			*Me*
	11.7			C_5Me_5
1d, Cp*IrNDIPP	143.5			Ph
	128.3			Ph[c]
	123.9			Ph
	122.4			Ph
	85.0			C_5Me_5
	28.2			$CHMe_2$
	22.6			$CHMe_2$
	8.8			C_5Me_5
3a, Cp*Ir(*t*-BuNH$_2$)Cl$_2$[f]	85.4			C_5Me_5
	54.3			CMe_3
	31.3			CMe_3
	9.6			C_5Me_5
3d, Cp*Ir(DIPPNH$_2$)Cl$_2$[f]	139.5			Ph
	136.6			Ph
	125.7			Ph
	123.6			Ph
	85.8			C_5Me_5
	27.4			$CHMe_2$
	23.3			$CHMe_2$
	8.6			C_5Me_5
4, Cp*Ir(CN*t*-Bu)-(*t*-BuNCN*t*-Bu)	138.6			terminal *CN*
	137.8			bridging *CN*
	95.0			C_5Me_5
	56.0			CMe_3
	55.3			CMe_3
	54.0			CMe_3
	32.3			CMe_3
	31.5			CMe_3
	28.3			CMe_3
	9.8			C_5Me_5
5a, Cp*Ir(CO)(*t*-BuNCO)	174.7			*CO*
	143.5			*t*-BuN*CO*
	98.8			C_5Me_5
	53.8			CMe_3
	28.6			CMe_3
	9.6			C_5Me_5
5b, Cp*IrPPh$_3$(*t*-BuNCO)	140.7	d	7.2	*CO*
	134.8	d	10.9	*o*- or *m*-P*Ph*$_3$
	134.4	d	51.6	ipso P-*Ph*
	129.3			*p*-P-*Ph*
	127.7	d	10	*o*- or *m*-P-*Ph*[c]
	92.9	d	3.5	C_5Me_5
	48.8			CMe_3
	29.1			CMe_3
	10.1			C_5Me_5
6, Cp*IrN*t*-Bu(dppePt)[d]	138.8–137.6	m		ipso P*Ph*
	137.6–136.5	m		ipso P*Ph*
	135.6	m		*o*- or *m*-P*Ph*
	134.1	m		*o*- or *m*-P*Ph*
	130.2			*p*-P*Ph*
	129.7			*p*-P*Ph*
	128.6	m		*o*- or *m*-P*Ph*[e]
	128.5	m		*o*- or *m*-P*Ph*[e]
	83.8			C_5Me_5
	70.0	dd	8.9, 2.5	CMe_3
	34.4–33.7	m		PCH_2[e]
	34.3			CMe_3[e]
	33.0–32.2	m		PCH_2
	12.3			C_5Me_5
7a, Cp*Ir(N*t*-BuOCO)	170.9			CO_2
	83.9			C_5Me_5
	56.6			CMe_3
	31.8			CMe_3
	10.4			C_5Me_5
7b, Cp*IrPPh$_3$(N*t*-BuOCO)	166.6			CO_2
	134.8	d	10.2	*o*- or *m*-P*Ph*$_3$
	132.8	d	51.8	ipso P*Ph*$_3$
	130.1			Ph
	128.5			Ph[c]
	91.3			C_5Me_5
	51.3			CMe_3
	32.5			CMe_3
	9.3			C_5Me_5
8, Cp*Ir(RCCRN-*t*-BuRCCR) (R = CO_2Me)	169.3			*CO*
	166.6			*CO*
	93.4			C_5Me_5
	78.4			C=C
	66.6			C=C
	52.6			CMe_3
	52.4			CO_2Me
	50.6			CO_2Me
	27.2			CMe_3
	8.5			C_5Me_5
9a, Cp*Ir(N*t*-BuC(O)-CH=CHCO$_2$)[b]	168.0			*CO*
	161.7			*CO*
	94.9			C_5Me_5
	83.3			*CH*
	83.0			*CH*
	54.4			CMe_3
	31.5			CMe_3
	10.0			C_5Me_5
9b, Cp*Ir(CO)(N*t*-BuC-(O)CH=CHCO$_2$)	184.2			*CO*
	183.0			*CO*
	169.2			*CO*
	141.0			*CH*
	137.3			*CH*
	99.7			C_5Me_5
	57.5			CMe_3
	33.9			CMe_3
	9.1			C_5Me_5

[a] All spectra in C_6D_6 at 20 °C unless indicated. [b] Acetone-d_6. [c] Partially obscured by solvent. [d] THF-d_8. [e] Overlapping peaks. [f] CD_2Cl_2.

The reaction of the readily available dimer $[Cp^*IrCl_2]_2$ with lithium amides is a general, high-yield method for the preparation of the monomeric imido compounds reported here. A plausible mechanism for these reactions is initial formation of the bisamide complex $Cp^*Ir(NHR)_2$ followed by α-elimination of amine. The isoelectronic chelating bisamide complex $Cp^*Rh(o\text{-}C_6H_4(NH)_2)$ has been prepared by the deprotonation of *o*-phenylenediamine in the presence of $[Cp^*RhCl_2]_2$.[16] The proposed α-elimination is a common route to metal–ligand multiple bonds.[17] Alternatively, dehydrohalogenation of the intermediate Cp*Ir(NHR)(Cl)

(15) Imido complexes of group 9–11 transition metals: for dimeric μ_2 bridging complexes, see: ref 6 and (a) Meij, R.; Stufkens, D. J.; Vrieze, K.; Brouwers, A. M. F.; Overbeek, A. R. *J. Organomet. Chem.* **1978**, *155*, 123. (b) Ge, Y.-W.; Sharp, P. R. *J. Am. Chem. Soc.* **1990**, *112*, 3667 and references therein. For μ_3-bridging trimeric clusters, see: (c) Otsuka, S.; Nakamura, A.; Yoshida, T. *Inorg. Chem.* **1968**, *7*, 261. (d) Muller, J.; Dorner, H.; Kohler, F. H. *Chem. Ber.* **1973**, *106*, 1122. (e) Abel, E. W.; Blackmore, T.; Whitley, R. S. *Inorg. Nucl. Chem. Lett.* **1974**, *10*, 941. (f) Gall, R. S.; Connelly, N. G.; Dahl, L. F. *J. Am. Chem. Soc.* **1974**, *96*, 4017. (g) Bedard, R. L.; Dahl, L. F. *J. Am. Chem. Soc.* **1986**, *108*, 5942. (h) Wakatsuki, Y.; Okada, T.; Yamazaki, H.; Cheng, C. *Inorg. Chem.* **1988**, *27*, 2958.

(16) Espinet, P.; Bailey, P. M.; Maitlis, P. M. *J. Chem. Soc., Dalton Trans.* **1979**, 1542.

(17) Reference 1a, pp 52–112.

by the strong base LiNHR could form **1a–d**. A similar process occurs in the reaction of $Cp^*_2Zr(SH)(I)$ with $KN(SiMe_3)_2$ to give $Cp^*_2Zr{=}S$, which can be trapped by dative ligands.[18]

Consistent with these ideas, synthesis and dehydrohalogenation of the amine coordination compounds $Cp^*Ir(RNH_2)Cl_2$ was also used to prepare compounds **1a** and **1d**. This route to imido compounds requires an extra step and proceeds in lower yield than the method described above, but does not result in the formation of amine byproduct. This is convenient when dealing with the involatile arylamines.

The arylimido complexes **1c,d** were also synthesized from *tert*-butylimido compound **1a** by exchange with the appropriate arylamines. Similar reactions have been reported for preparation of imido complexes from oxo precursors as in the reaction of OsO_4 with t-$BuNH_2$ to give H_2O and $OsO_3N$$t$-Bu.[19] We suggest that these reactions proceed by initial coordination of the entering amine to the metal center, followed by proton transfer to give the intermediates $Cp^*Ir(NH$$t$-$Bu)(NHAr)$. These then undergo α-elimination of *tert*-butylamine to give the observed products. The related species $Cp_2Zr{=}N$$t$-Bu reacts with *tert*-butylamine to give stable $Cp_2Zr(NH$$t$-$Bu)_2$, providing a model for the addition phase of this reaction.[4a] Similarly, the methylene complex $Cp^*IrPMe_3(CH_2)$ adds a variety of acids HX across the Ir–C double bond to give the stable products $Cp^*IrPMe_3(Me)(X)$.[20]

Molecular and Electronic Structures of the Imido Compounds. Linear M–N–C angles are usually taken as evidence that the imido ligand acts as a four-electron donor to the metal center.[21] For **1a–d** the Ir–N–C(Si) angles range from 177.2 (5)° to 170.8 (2)°, so these can be classified as 18-electron compounds with an Ir–N triple bond. The short Ir–N distances in **1a–d** (ranging from 1.712 (7) Å to 1.750 (3) Å) are consistent with this description of the bonding. They are also in reasonable agreement with Nugent and Haymore's predicted Ir≡N triple bond length of 1.68 Å, derived from Pauling's relative metallic sizes and the typical Re≡N triple bond length of 1.69 Å.[22] Complex **1a** does not form stable adducts (with, for example, PPh_3 or MeCN) which would allow localization of the Ir–N bonding electrons on nitrogen. Similarly, delocalization of electron density away from iridium toward silicon does not seem to occur in **1b**; the N–Si distance of 1.715 (3) Å is typical of a single bond.[23]

We have only succeeded in isolating terminal imido compounds Cp^*IrNR with bulky R groups. Attempts to prepare analogous complexes with other R groups (e.g., Ph and $SiPh_3$) led only to intractable materials. In the isolable complexes, steric effects apparently prevent formation of imido-bridged dimers $[Cp^*IrNR]_2$. The isoelectronic complex with the smaller oxo ligand exists as the dimer $[Cp^*IrO]_2$, which was suggested to have an Ir–Ir double bond to explain its intense red color and observed reactivity.[6]

Unlike previously reported metal imides which have metal electron configuration d^4 or less, complexes **1a–d** formally have six metal d electrons. The fact that terminal oxo and imido compounds of the late transition metals had not previously been prepared had been rationalized with a molecular orbital argument[24a] that utilized an octahedral $L_5M{=}X$ (X = O or N–R) complex as a model. In this model two d orbitals (d_{z^2} and $d_{x^2-y^2}$) lie at relatively high energies because of the usual antibonding

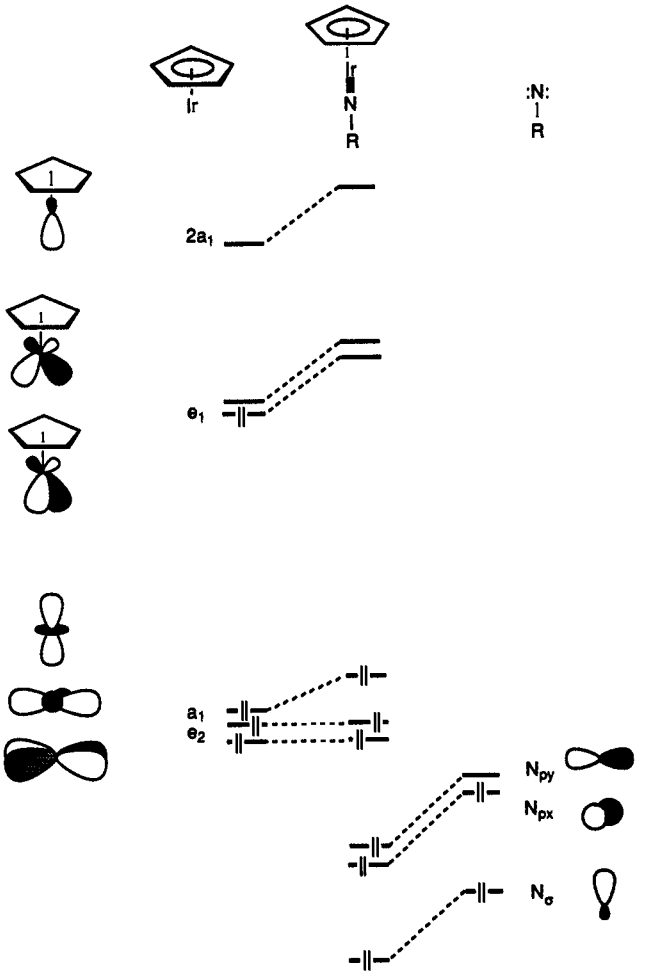

Figure 4. Molecular orbital diagram showing interaction of CpM and RN fragments to give energy level pattern for CpMNR.

interactions between these orbitals and the L donor orbitals. At the same time, the e set d_{xz} and d_{yz} are raised in energy because of their antibonding interactions with the p orbitals of the X ligand. This leaves only one predominantly d orbital (d_{xy}), lying in the L_4 plane, at the nonbonding level, and so $L_5M{=}X$ (X = O, NR) complexes are predicted to be unstable when they have more than two d electrons.[24a]

There are substantial differences between the $L_5M{=}X$ and $CpM{=}X$ systems that provide a way for the latter to escape the destabilizing influences that Mayer has identified for $L_5M{=}X$. Figure 4 illustrates a qualitative molecular orbital diagram that describes the interaction of a CpM fragment[24b] with an NR ligand. In the CpM fragment the two highest lying orbitals (e_1) are combinations formed by antibonding interactions between the bonding Cp e set and the metal d_{xz} and d_{yz} orbitals. The absence of ligands in the xy plane allows d_{xy} and $d_{x^2-y^2}$ to remain nonbonding, along with d_{z^2}, which calculations show does not interact strongly with the Cp ligand orbitals.[24b] Allowing the σ and p orbitals from the R–N fragment to interact with CpM generates a σ-bond by interaction of N_σ with the d_{z^2} and high-lying $2a_1$ orbitals (we assume both will be raised in energy, although significant involvement of $2a_1$ in this mixture will tend to contribute to maintaining nonbonding character in d_{z^2}). In analogy to the $L_5M{=}X$ system,[24a] two π bonds are formed by interaction of the nitrogen p_x and p_y orbitals with the high-lying e_1 levels. A total of six bonding Cp electrons (not shown), eight d electrons, and four nitrene electrons fills the bonding and approximately nonbonding levels of $CpM{=}NR$, leading to an essentially closed shell structure. From the way the electrons are used to fill CpM, RN, and $CpM{=}NR$, one concludes that there is substantial transfer of electron density from the CpM e_1 set into the nitrogen p system. This supports a qualitative picture of the complex as having a triple

(18) Carney, M. J.; Walsh, P. J.; Bergman, R. G. *J. Am. Chem. Soc.* **1990**, *112*, 6426.

(19) For exchange reactions of oxo compounds with amines, see ref 3b and references therein. In this case, reaction of $[Cp^*IrO]_2$ with t-$BuNH_2$ does not give **1a** and water; instead, an unidentified red material is formed (Foo, T.; Bergman, R. G., unpublished results). The same red compound is produced by the reaction of **1a** with H_2O.

(20) Klein, D. P.; Bergman, R. G. *J. Am. Chem. Soc.* **1989**, *111*, 3079.

(21) See ref 1a, pp 22–23. For a recent counterexample, see: Anhaus, J. T.; Kee, T. P.; Schofield, M. H.; Schrock, R. R. *J. Am. Chem. Soc.* **1990**, *112*, 1643.

(22) Reference 1b, p 134.

(23) Brennan, J. G.; Andersen, R. A.; Zalkin, A. *J. Am. Chem. Soc.* **1988**, *110*, 4554 and references therein.

(24) (a) Mayer, J. M. *Comments Inorg. Chem.* **1988**, *8*, 125. (b) Albright, T. A.; Burdett, J. K.; Whangbo, M.-H. *Orbital Interactions in Chemistry*; Wiley-Interscience: New York, 1985; pp 387–389.

bond and a formally d^6, Ir(III) electron configuration.

Nucleophilicity of Cp*IrN*t*-Bu. For *tert*-butylimido compounds of the early transition metals, decreasing electron density on the imido nitrogen causes a downfield shift of the α-C resonance and an upfield shift in the β-C resonance in the ^{13}C NMR spectrum. The difference $\Delta = \delta(\alpha) - \delta(\beta)$ can provide a qualitative measure of electron density on nitrogen. The trend in Δ values often parallels reactivity; the electrophilic OsO_3N*t*-Bu has $\Delta = 55$, while for the nucleophile PPh_3N*t*-Bu $\Delta = 16$.[25] The Δ value of 29 for **1a** is difficult to interpret in the absence of data for other monomeric late transition-metal imido complexes.

Experimentally, we find that Cp*IrN*t*-Bu is a modest nucleophile compared with other bases (e.g., it reacts with methyl iodide and anhydrides but is unreactive toward simple ester functions such as those in MeO_2CCCCO_2Me), but it is unusually nucleophilic compared with other known molecules in its class. In metal–imido complexes that have been prepared previously, the nitrogen lone pair is tied up in the M–N triple bond and is inert to alkylating agents. The reaction of $Mo(NAr)_2(S_2CNEt_2)_2$ with MeBr to give $Mo(NAr)Br_2(S_2CNEt_2)_2$ and $ArNMe_3Br$ is a rare exception to this generalization; one imido ligand in the starting material, however, does not react with MeBr.[26] The observed nucleophilicity of **1a** is not simply an effect of the late transition metal: the imido ligand in the transient species $[Ir(NH_3)_5NH]^{3+}$ reacts as a strong electrophile.[27]

Coupling of Cp*IrN*t*-Bu with CO and CN*t*-Bu. The coupling reactions of **1a** with carbon monoxide and *tert*-butyl isocyanide show similarities to those of nitrenes (NR). The free nitrene NCO_2Et reacts with CN*t*-Bu to form the carbodiimide $EtO_2CN{=}C{=}N$*t*-Bu.[28] Azides ArN_3 have been reported to react at 160–180 °C under 200–300 atm CO to form aryl isocyanates, presumably via the free nitrene ArN.[29]

Carbodiimides were reported previously from coupling of *t*-BuNC with NPh, formed by deoxygenation of coordinated PhNO at a nickel center.[30] Imido ligands in clusters can be carbonylated to yield isocyanates,[31] but this usually requires high temperatures and pressures. Sharp's μ_2-imido/amido complex $Rh_2(\mu\text{-}NR)(CO)_2(\mu\text{-dppm})_2$ reacts with CO under mild conditions to give sequentially a bridging isocyanate ligand and then a dimetallocyclodiimide.[32] The transformations of **1a** to **5a,b** reported here are the first carbonylations of a terminal imido ligand to give isocyanate complexes.

The selective formation of Cp^*IrPPh_3(*t*-BuNCO) (**5b**) from Cp*IrN*t*-Bu (**1a**) and 1 equiv of PPh_3 proceeds under an atmosphere of CO. Control experiments show that neither **1a** nor **5a** reacts with PPh_3. Further, when **5a** is added to a mixture of **1a** and PPh_3 and CO is added, **5a** is unaffected while **1a** is smoothly transformed to **5b**. These observations are consistent with either of the mechanisms shown in Scheme V: intermediacy of the 16-electron species Cp*Ir(*t*-BuNCO), which is trapped preferentially by PPh_3, or direct attack on the 18-electron Cp*Ir(N*t*-Bu)(CO) by ligand CO or PPh_3 to induce N–C bond formation.

Reactions of the Iridium–Nitrogen Multiple Bond and Cycloadditions. Stone and co-workers showed that metal carbenes and carbynes as well as metal–metal bonded species displace ethylene from $L_2Pt(C_2H_4)$ (L = PR_3) to form new compounds that may be described as π-complexes of the L_2Pt fragment or as, for example, bridging carbene compounds.[33] The reaction of

Scheme V

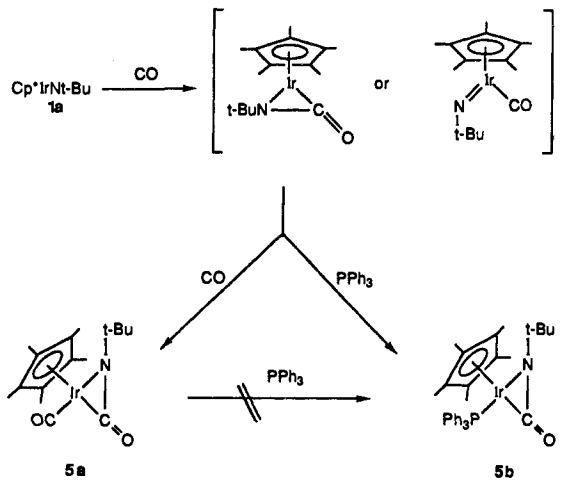

Scheme VI

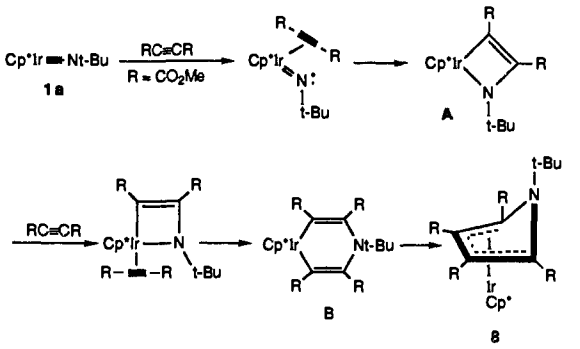

Cp*IrN*t*-Bu with $dppePt(C_2H_4)$ to give Cp*IrN*t*-Bu(dppePt) (**6**) is the first extension of this approach to metal–nitrogen multiple bonds. According to the $^{31}P\{^1H\}$ NMR spectrum, the iridium–imido moiety is bound asymmetrically to Pt, so **6** is probably best described as a heterobimetallic compound with a bridging imido ligand. Unfortunately, **6** did not form crystals suitable for X-ray diffraction, so the detailed nature of the Ir–N, Pt–N, and Ir–Pt bonding could not be determined.

Metal carbenes are well-known to undergo [2 + 2] cycloadditions with unsaturated substrates to form metallacycles,[34] but this is a novel type of reaction for metal–imido complexes. Recently, formation of metallacycles has been observed in the reaction of alkynes with imidozirconocene complexes.[4a] The reaction of **1a** with carbon dioxide gave the metallacycle Cp*Ir(N*t*-BuC(O)O) (**7a**). This is a net 2 + 2 cycloaddition, but we do not yet know if this term provides an accurate mechanistic description of the process. The fact that only relatively electrophilic substrates react with Cp*IrN*t*-Bu suggests (as a referee has pointed out) that in analogy to the CH_3I and anhydride reactions these processes may be initiated by nucleophilic attack of nitrogen at an electrophilic carbon. A related transformation was recently observed in the reaction of the carbene complex $Cp^*IrPMe_3(CH_2)$ with CO_2 to give $Cp^*IrPMe_3(CH_2OCO)$.[20]

The crystal structure of **7a** is consistent with a decrease in Ir–N bond order and a change in hybridization at nitrogen from sp to sp^2. This "bifunctional" activation of carbon dioxide[35] suggests that **1a** contains iridium acting as a Lewis acid in addition to nitrogen acting as a Lewis base. Metallacycle **7a** is formally a 16-electron species, but donation of the N and O lone pair electrons

(25) (a) Reference 1b, pp 143–4. (b) Nugent, W. A.; McKinney, R. J., Kasowski, R. V.; Van-Catledge, F. A. *Inorg. Chim. Acta* **1982**, *65*, L91.
(26) Maatta. E. A.; Wentworth, R. A. D. *Inorg. Chem.* **1979**, *18*, 2409.
(27) Lane, B. C.; McDonald, J. W.; Basolo, F.; Pearson, R. G. *J. Am. Chem. Soc.* **1972**, *94*, 3786.
(28) Lwowski, W. In *Nitrenes*; Lwowski, W., Ed.; Wiley-Interscience: New York, 1970; p 216.
(29) Bennett, R. P.; Hardy, W. B. *J. Am. Chem. Soc.* **1968**, *90*, 3295.
(30) Otsuka, S.; Aotoní, Y.; Tatsuno, Y.; Yoshida, T. *Inorg. Chem.* **1976**, *15*, 656.
(31) For a review, see: Han, S. H.; Geoffroy, G. L. *Polyhedron* **1988**, *7*, 2331.
(32) Ge, Y.-W.; Sharp, P. R. *Organometallics* **1988**, *7*, 2234.
(33) For reviews, see: (a) Stone, F. G. A. *Inorg. Chim. Acta* **1981**, *50*, 33. (b) Stone, F. G. A. *Acc. Chem. Res.* **1981**, *14*, 318.
(34) Collman, J. P.; Hegedus, L. S.; Norton, J. R.; Finke, R. G. *Principles and Applications of Organotransition Metal Chemistry*; University Science Books: Mill Valley, CA, 1987; Chapter 16, and references therein.
(35) For a recent example, see: Gambarotta, S.; Floriani, C.; Chiesi-Villa, A.; Guastini, C. *J. Am. Chem. Soc.* **1985**, *107*, 2985. For other references, see: (a) Darensbourg, D. J.; Kudaroski, R. A. *Adv. Organomet. Chem.* **1983**, *22*, 129. (b) Ziessel, R. *Nouv. J. Chim.* **1983**, *7*, 613. (c) Behr, A. *Angew. Chem., Int. Ed. Engl.* **1988**, *27*, 661.

to the Ir center may provide some Ir–N or Ir–O double bond character which stabilizes the unsaturated metal center. However, **7a** reacts immediately with PPh_3 to form the coordinatively saturated adduct $Cp^*IrPPh_3(N$*t*-$BuC(O)O)$ (**7b**).

The O_2CNR ligand has previously been prepared by another apparent 2 + 2 cycloaddition between a metal oxo group and an organic isocyanate: $Cp_2Mo{=}O$ reacts with PhNCO to give the metallacycle $Cp_2Mo(O_2CNPh)$.[36] The iridium oxo complex $[Cp^*IrO]_2$ reacts with *t*-BuNCO, providing an alternate route to **7a**, as shown in Scheme III.[12]

The oxo compound Cp^*ReO_3 reacts with 2 equiv of alkyne in the presence of PPh_3 to give the "rhenapyran" $Cp^*Re(O)(RC{=}CROCR{=}CR)$.[37] As Herrmann recently predicted that this reaction could be extended to imido compounds,[38] we originally formulated the product of the reaction of **1a** with dimethylacetylenedicarboxylate as the alkylated metallapyridine $Cp^*Ir(RC{=}CRN$*t*-$BuCR{=}CR)$ (species B in Scheme VI). The crystal structure of this compound, however, showed that it is the pyrrole complex **8**, which is formally related to the metallapyridine by a C–C reductive elimination. A possible mechanism leading to the formation of **8** is shown in Scheme VI. The first step involves complexation of the alkyne to Ir, accompanied by localization of the N lone pair on nitrogen. The next step, formation of four-membered metallacycle A, is precedented in the $Cp_2Zr{=}N$*t*-Bu system, in which such compounds are stable.[4a] Complexation of another alkyne followed by a second apparent 2 + 2 cycloaddition gives the metallapyridine B, analogous to the rhenapyran. Finally, C–C reductive elimination leads to the observed product.

Although 2-butyne and 1-phenylpropyne do not react with **1a** even on heating, this reaction with an activated alkyne to give **8** results in the formation of two N–C bonds and a C–C bond in one pot. Other metal complexes have been used to promote or catalyze related "2 + 2 + 1" reactions resulting in the formation of five-membered rings. For example, pyrroles have been prepared by the reaction of cobaltacyclopentadienes and organic azides.[39] The rhenium–oxo compound described above reacts with alkynes to give furans, and a CpCo-catalyzed synthesis of thiophenes from sulfur and alkynes has been described.[40] Intermediates with metal–ligand multiple bonds may be important in such reactions but are usually not detected; the conversion of stable imido complex **1a** to **8** is the first case in which conversion of a metal-bound nitrene to a pyrrole can be directly observed.

Summary. The metathesis of $[Cp^*IrCl_2]_2$ with lithium amides is a general, high yield route to the monomeric imido compounds Cp^*IrNR, if bulky R groups are employed. Dehydrohalogenation of the amine coordination complexes $Cp^*Ir(RNH_2)Cl_2$ with $KN(SiMe_3)_2$ and exchange of arylamines with Cp^*IrN*t*-Bu also yields the imido complexes. These synthetic methods are similar to those employed for known imido compounds, suggesting that other late transition-metal imido (or phosphinidene) complexes can be prepared.

The compound Cp^*IrN*t*-Bu has a moderately reactive M–N bond. It undergoes novel reactions with electrophiles in which the N*t*-Bu group acts as a nucleophile, resulting in N–C bond formation with the substrates MeI, CO, and CN*t*-Bu. The Ir–N multiple bond undergoes some reactions reminiscent of metal–carbene and –carbyne chemistry, such as its addition to dppePt and apparent 2 + 2 cycloadditions with CO_2 and an alkyne.

Previous work in this group has shown that the Cp^*Ir fragment can support oxo and carbene ligands. In comparison to $[Cp^*IrO]_2$ and $Cp^*IrPMe_3(CH_2)$, the imido compounds described here are unique in forming monomers stable at room temperature. We suggest that this kinetic stabilization is due in part to an essentially closed-shell electronic structure and in part to the use of bulky R groups. The multiply bonded groups in these complexes are nucleophilic, perhaps due to the ability of the Cp^*Ir center to stabilize developing positive charge. The observation of cycloaddition reactions of **1a** suggests that the rich cycloaddition/metathesis-based chemistry of the metal–carbon multiple bond may also be accessible for metal–imido compounds.

Experimental Section

General Methods. Unless otherwise noted, all reactions and manipulations were performed in dry glassware under nitrogen atmosphere in a Vacuum Atmospheres 553-2 drybox equipped with an M6-40-1H Dri-train or using standard Schlenk techniques.

All ^1H, ^{13}C, ^{15}N, and ^{31}P NMR spectra were recorded on 300-, 400-, or 500-MHz instruments at the University of California, Berkeley NMR facility. The 300-MHz instrument was constructed by Rudi Nunlist and interfaced with a Nicolet 1280 computer. The 400- and 500-MHz machines were commercial Bruker AM series spectrometers. ^1H and ^{13}C NMR chemical shifts are reported in parts per million downfield from tetramethylsilane. ^{31}P NMR chemical shifts are given in parts per million downfield from 85% H_3PO_4. Coupling constants are given in Hz. Infrared spectra were recorded on a Perkin-Elmer Model 1550 Fourier transform spectrometer. Infrared bands are reported in cm^{-1}. Melting points are uncorrected and were determined with a Thomas-Hoover Unimelt capillary melting point apparatus. Elemental analyses were conducted by the U.C. Berkeley Microanalysis Facility, and mass spectra were recorded by the U.C. Berkeley Mass Spectrometry Laboratory on AEI-MS12 and Kratos MS-50 instruments.

Benzene, toluene, and THF were distilled from sodium/benzophenone, pentane was distilled from lithium aluminum hydride, and acetone was dried over 4Å molecular sieves. *tert*-Butyl isocyanide and dimethylacetylenedicarboxylate were distilled from phosphorus pentoxide, and *tert*-butylamine, arylamines, and hexamethyldisiloxane were distilled from calcium hydride. H_2NSiMe_2*t*-Bu was made from NH_3, and $ClSiMe_2$*t*-Bu was prepared by the literature method;[41] lithium amides were prepared from amines by using *n*-butyllithium in toluene. Methyl iodide was dried over molecular sieves and stored in the dark over copper wire. Maleic anhydride was recrystallized from chloroform, and triphenylphosphine was recrystallized from pentane. $[Cp^*IrCl_2]_2$ was prepared by a literature method,[5] and $dppePt(C_2H_4)$ was prepared by a modification of the literature method: the reducing agent used was $NaBH_4$ in ethanol, rather than sodium naphthalide in THF.[42] $KN(SiMe_3)_2$ was prepared in THF from KH and the amine, which was dried over CaH_2. Unless otherwise noted, all other reagents were used as received from commercial suppliers. Reactions with gases involved condensation of a calculated pressure (ideal gas law) of gas from a bulb of known volume into the reaction vessel at −196 °C. Unless noted otherwise, all reactions were done at ambient temperature.

Cp^*IrN*t*-Bu (1a). A 100-mL flask was charged with $[Cp^*IrCl_2]_2$ (1.00 g, 1.26 mmol), LiNH*t*-Bu (420 mg, 5.32 mmol), and a stir bar. THF (50 mL) was condensed into the flask at −196 °C. The flask was placed in an ice bath, and the THF was allowed to thaw with stirring. Within 5 min the orange slurry became homogeneous, and the solution turned dark brown-yellow. The volatile materials were removed in vacuo with the flask still in the ice bath. The brown-yellow residue was extracted with pentane and filtered through Celite on a frit to give a dark orange-brown solution. Removal of the pentane in vacuo gave 914 mg of yellow powder (91%), pure according to ^1H NMR spectroscopy. Yellow crystals suitable for analysis were obtained by recrystallization from pentane at −40 °C. The compound can also be sublimed readily with gentle heating from a hot water bath. It rapidly darkens and turns brown in the solid state, even under nitrogen, although this does not change its ^1H NMR spectrum. It is best stored at −40 °C in the dark. GC analysis of the volatile products in a smaller scale reaction confirmed the formation of *tert*-butyl amine in 56% yield, by integration against a cyclohexane standard: mp 95–100 °C dec; IR (KBr) 2975, 2910, 1258 (s), 1071, 1033 cm^{-1}; MS (EI) *m/e* 399/397 (M^+, $^{193}Ir/^{191}Ir$), 384/382 $(M - Me)^+$, 343/341 (base, $^{193}Ir/^{191}Ir$). Anal. Calcd for $C_{14}H_{24}IrN$: C, 42.18; H, 6.08; N, 3.51. Found: C, 42.22; H, 5.92; N, 3.45.

X-ray Crystal Structure Determination of 1a. Clear yellow blocky crystals were obtained from pentane at −40 °C. Fragments cleaved from some of these crystals were mounted on glass fibers by using polycyanoacrylate cement and then coated with epoxy to protect them from the air. Preliminary precession photographs indicated orthorhombic Laue symmetry and yielded approximate cell dimensions. The crystal used for data collection was then transferred to our Enraf-Nonius CAD-4 diffractometer and centered in the beam.[43] Automatic peak search and

(36) Jernakoff, P.; Geoffroy, G. L.; Rheingold, A. L.; Geib, S. J. *J. Chem. Soc., Chem. Commun.* **1987**, 1610.
(37) de Boer, E. J. M.; de With, J.; Orpen, A. G. *J. Am. Chem. Soc.* **1986**, *108*, 8721.
(38) Herrmann, W. A. *Angew. Chem. Int. Ed. Engl.* **1988**, *27*, 1297.
(39) Hong, P.; Yamazaki, H. *J. Organomet. Chem.* **1989**, *373*, 133.
(40) Bonnemann, H.; Brijoux, W. *New J. Chem.* **1987**, *11*, 549.
(41) Bowser, J. R.; Neilson, R. H.; Wells, R. L. *Inorg. Chem.* **1978**, *17*, 1882.

indexing procedures yielded the orthorhombic reduced primitive cell. The final cell parameters and specific data collection parameters are given in Table I.

The 2248 raw intensity data were converted to structure factor amplitudes and their esd's by correction for scan speed, background, and Lorentz and polarization effects. Inspection of the intensity standards revealed a nonlinear reduction of about 5% of the original intensity. The data were corrected for this decay. Inspection of the azimuthal scan data showed a variation $I_{min}/I_{max} = 0.395$ for the average curve. Since the crystal shape was obscured by the epoxy, an empirical correction based on the observed variation was applied to the data ($T_{max} = 1.0$, $T_{min} = 0.40$). Inspection of the systematic absences indicated possible space groups $Pca2_1$ and $Pbcm$. The choice of $Pbcm$ was confirmed by the successful solution and refinement of the structure (while data were actually collected in the acentric setting, they are reported as if collected in the centric setting). Removal of systematically absent and averaging of redundant data ($R(I) = 3.5\%$) left 1053 unique data in the final data set.

The structure was solved by Patterson methods and refined via standard least-squares and Fourier techniques. In a difference Fourier map calculated following the refinement of all non-hydrogen atoms with anisotropic thermal parameters, peaks were found corresponding to the positions of most of the hydrogen atoms. Hydrogen atoms were assigned idealized locations and values of B_{iso} approximately 1.3 times the B_{eqv} of the atoms to which they were attached. They were included in structure factor calculations but not refined.

The final residuals for 83 variables refined against the 873 data for which $F^2 > 3\sigma(F^2)$ were $R = 2.06\%$, wR = 2.60% and GOF = 1.168. The R value for all 1053 data was 3.32%. In the final cycles of refinement a secondary extinction parameter was included (maximum correction—20% on F). The quantity minimized by the least-squares program was $\sum w(|F_o| - |F_c|)^2$, where w is the weight of a given observation. The p factor, used to reduce the weight of intense reflections, was set to 0.03 throughout the refinement. The analytical forms of the scattering factor tables for the neutral atoms were used, and all scattering factors were corrected for both the real and imaginary components of anomalous dispersion. Inspection of the residuals ordered in ranges of $\sin\theta/\lambda$, $|F_o|$, and parity and value of the individual indexes showed no unusual features or trends. The largest peak in the final difference Fourier map had an electron density of 0.56 $e^-/Å^3$ and the lowest excursion −0.65 $e^-/Å^3$.

t-Bu^{15}NH$_3$Cl. This compound was prepared by the method of Gilchrist and Collum,[44] with slight modifications. Pivaloyl chloride (3.0 mL, 24 mmol) in 10 mL of Et_2O was layered onto a solution of $^{15}NH_4Cl$ (997 mg, 18.3 mmol) in 3.75 mL of H_2O in a 25-mL pear-shaped flask so the layers did not mix. The flask was cooled in an ice bath, and NaOH (4.28 g, 107 mmol) in 5 mL of water was added by pipet to the aqueous layer, with slow stirring by a flea-sized stir bar to avoid mixing the layers. The flask was warmed to room temperature, stirred for 15 min, then capped with a glass stopper, and shaken several times, with venting. A white precipitate formed and was collected by filtration on a coarse frit. The white solid was extracted with 100 mL of CH_2Cl_2 in several portions, and the solvent was removed with a rotary evaporator to yield 1152 mg of white solid [^{15}N]-pivalamide, mp 148–152 °C (lit. mp 154–157 °C). An additional 345 mg of product (mp 156–158 °C) was obtained by removing the solvent from the filtrate above and identical workup: total yield 1.50 g (80%). This material was used directly in the next step.

A 20% aqueous KOH solution (40.5 mL) in a 250-mL Erlenmeyer flask was cooled in an ice bath. Bromine (1125 μL, 3.5 g, 22 mmol) was added via syringe, causing the solution to turn yellow. The pivalamide (1.50 g, 14.6 mmol) was added as a solid in several portions with stirring. The mixture was stirred at 0 °C for 90 min, during which time it became viscous and yellow, and then at room temperature for 20 min. The flask was cooled in an ice bath, and concentrated HCl was added cautiously in several portions (~35 mL total) until the solution was distinctly acidic, homogeneous, and orange. The flask was heated to 50 °C for 15 min and then cooled to 0 °C. Ether (45 mL) was added, and the mixture was made distinctly basic by the addition of KOH pellets. As the addition proceeded, the mixture bubbled, the ether layer remained orange, and the aqueous layer became milky white. When the solution was basic, the ether layer had become light yellow. The ether layer was collected, and the aqueous layer was washed with three 20-mL portions of ether. The ether layers were combined, dried over K_2CO_3, and poured into a 250-mL, three-necked flask which was cooled to 0 °C. Gaseous HCl was bubbled into the flask with stirring, causing the solution to turn orange and then yellow, while white precipitate formed. The white solid t-Bu $^{15}NH_3Cl$ was collected by filtration with a Buchner funnel and washed with ether. The solid was placed under high vacuum for 1 h to give 1.12 g of the hydrochloride (75%): ^{1}H NMR (D_2O) δ 1.20 (d, J = 2.8). This material was used directly in the next step.

Li^{15}NHt-Bu and Cp*Ir^{15}Nt-Bu ([^{15}N]-1a). The ^{15}N hydrochloride (1.12 g, 10.1 mmol) was slurried in 20 mL of pentane in a Schlenk flask cooled to −78 °C, n-BuLi (15 mL of a 1.6 M hexane solution, 24 mmol) was added via cannula under nitrogen over a few minutes, with stirring. The suspension bubbled and became light yellow. The mixture was allowed to warm to room temperature; after 2 h the solvent was removed in vacuo to give a yellow oil. Addition of Et_2O to the oil caused the precipitation of a white powder, which was collected on a frit and washed with ether to give 960 mg of white solid (78% yield by mass balance); ^{1}H NMR (THF-d_8) δ 1.06 (d, J = 1.6, 9 H), −1.68 (d, J = 51, 1 H). This material also contained trace amounts of impurities according to ^{1}H NMR (and presumably LiCl as well). It was used in slight excess (mole ratio 5.5Li^{15}NHt-Bu:1[Cp*IrCl$_2$]$_2$) to prepare Cp*Ir^{15}Nt-Bu ([^{15}N]-1a) as described above: IR (KBr) identical with 1a except the peak at 1258 cm^{-1} shifts to 1240 cm^{-1}; ^{1}H NMR (C_6D_6) identical with 1a except the triplet at δ 1.32 becomes a doublet with J_{NH} = 2.4.

Cp*IrNSiMe$_2t$-Bu (1b). A flask was charged with 789 mg (0.99 mmol) of [Cp*IrCl$_2$]$_2$, 560 mg of LiNHSiMe$_2t$-Bu (4.09 mmol), and a stir bar. THF (30 mL) was condensed onto the solids at liquid nitrogen temperature. The mixture was thawed in an ice bath with stirring. After ~1 min the orange slurry became a clear dark brown solution. After 5 min of stirring at 0 °C, the THF was removed in vacuo with the flask still in the ice bath, to give an orange-brown solid. This was placed under high vacuum overnight to remove excess silylamine. The residual solid was extracted with ~50 mL of pentane, and the pentane solution was filtered through Celite on a frit. Removal of the pentane from the filtrate in vacuo gave 814 mg (90%) of yellow crystalline solid. This material readily turns brown at room temperature in the drybox with no change in its NMR spectrum. Yellow crystals suitable for analysis were obtained by recrystallization from pentane at −40 °C: mp 75–80 °C dec; IR (KBr) 2950, 2923, 2894, 2851, 1241, 1117 (s), 832, 819, 803, 769, 675 cm^{-1}; Anal. Calcd for $C_{16}H_{30}IrNSi$: C, 42.07; H, 6.63; N, 3.07. Found: C, 42.18; H. 6.71; N, 3.05; MS (EI) m/e 457/455 (M$^+$), 400/398 (M − t-Bu)$^+$, base 74.

X-ray Crystal Structure Determination of 1b. Orange blocky crystals were obtained from pentane at −40 °C and mounted as described for 1a. X-ray data were collected as for 1a; the final cell parameters and specific data collection parameters are given in Table I.

The 1420 raw intensity data were reduced as for 1a. The data were corrected for a 33% decay in the intensity standards. An empirical absorption correction was applied to the data ($I_{min}/I_{max} = 0.81$). Inspection of the systematic absences indicated possible space groups $P2_1$ and $P2_1/m$. The choice of the centric group was confirmed by the successful solution and refinement of the structure. Removal of systematically absent and averaging of redundant data (R(I) = 1.4% for $0kl$ reflections) left 1309 unique data in the final data set.

The structure was solved by Patterson methods and refined via standard least-squares and Fourier techniques as for 1a (including treatment of the hydrogen atoms, except that values of $B_{iso} \sim 1.2B_{eqv}$ were used). Just prior to the final refinement, 11 reflections apparently affected by multiple diffraction were removed from the data set. The final residuals for 98 variables refined against the 1232 data for which $F^2 > 3\sigma(F^2)$ were $R = 1.61\%$, wR = 2.23%, and GOF = 1.663; the p factor was set to 0.02. The R value for all 1309 data was 1.92%. In the final cycles of refinement a secondary extinction parameter was included (maximum correction—15% on F). The largest peak in the final difference Fourier map had an electron density of 0.52 $e^-/Å^3$ and the lowest excursion −0.35 $e^-/Å^3$. Both were located near the Ir atom.

Cp*IrNXy (1c, Xy = 2,6-Me$_2$C$_6$H$_3$). A flask was charged with 495 mg (0.62 mmol) of [Cp*IrCl$_2$]$_2$, 330 mg (2.60 mmol) of LiNHXy, and a stir bar. THF (20 mL) was condensed into the flask at −196 °C and allowed to thaw at 0 °C with stirring. After 5 min the orange slurry had become homogeneous and yellow-brown. The THF was removed in vacuo with the reaction flask kept in the ice bath. The orange-brown residue was extracted with pentane, and the pentane solution was filtered through Celite on a frit to give a dark green-brown solution which was concentrated in vacuo until crystallization began (~2 mL) and cooled to −40 °C to give 183 mg (33%) of yellow-orange powder, which turns red-brown on standing: IR (KBr) 2913, 1411, 1381, 1372, 1336, 1095, 1033, 765 cm^{-1}; MS (EI) m/e 894/892 (2M$^+$), 772 (2M − XyNH)$^+$, 445 (M)$^+$, base 44. Anal. Calcd for $C_{18}H_{24}IrN$: C, 48.40; H, 5.43; N, 3.14. Found: C, 48.11; H, 5.59; N, 3.20.

(42) (a) Head, R. A. *J. Chem. Soc., Dalton Trans.* **1982**, 1637. (b) Polse, J.; Simpson, R. D.; Bergman, R. G., unpublished results.

(43) For a description of the X-ray diffraction and analysis protocols, see: (a) Hersh, W. H.; Hollander, F. J.; Bergman, R. G. *J. Am. Chem. Soc.* **1983**, *105*, 5834. (b) Cromer, D. T.; Waber, J. T. *International Table for X-ray Crystallography*; Kynoch Press: Birmingham, England, 1974; Vol. IV, Table 2.2B.

(44) Gilchrist, J.; Collum, D., unpublished results.

X-ray Crystal Structure Determination of 1c. Orange crystals grown from pentane at −40 °C were mounted as for **1a**. X-ray data were collected as for **1a**; the final cell parameters and specific data collection parameters are given in Table I.

The 2485 raw intensity data were reduced as above. The data were corrected for a 1.1% decay in the intensity standards. An empirical absorption correction based on the observed variation in the azimuthal scan data was applied: T_{max} = 1.0, T_{min} = 0.701. Inspection of the systematic absences indicated space group $I4_1/a$, confirmed by the successful refinement of the structure. Removal of systematically absent data left 2190 unique data in the final data set. The structure was solved by Patterson methods and refined via standard least-squares and Fourier techniques as for **1a** (except hydrogen atoms were not located or refined). Least-squares analysis of the data and correction for anomalous dispersion were carried out as for **1a**; the p factor was set to 0.03. The final residuals for 86 variables refined against the 1633 data for which $F^2 > 3\sigma(F^2)$ were R = 3.8%, wR = 4.5%, and GOF = 1.77. The R value for all 2190 data was 6.0%. The largest peak in the final difference Fourier map had an electron density of 1.26 e$^-$/Å^3 and the lowest excursion −0.86 e$^-$/Å^3.

Cp*Ir(*t*-BuNH$_2$)Cl$_2$ (3a). Into a flask containing [Cp*IrCl$_2$]$_2$ (0.35 g, 0.44 mmol) in 30 mL of CH_2Cl_2 was vacuum transferred 1.05 mmol of *tert*-butylamine. After the mixture was stirred for 5 min, the volatile materials were removed in vacuo. The residue was recrystallized from CH_2Cl_2/hexane at −20 °C to give red crystals, which were washed with hexane: yield 0.365 g in two crops (88%); IR (KBr) 3282, 3239, 2959, 1578, 1459, 1076, 1033, 810, 766 cm^{-1}. Anal. Calcd for $C_{14}H_{26}IrNCl_2$: C, 35.66; H, 5.56; N, 2.97. Found: C, 35.49; H, 5.58; N, 3.00.

Cp*IrN*t*-Bu via Cp*Ir(*t*-BuNH$_2$)Cl$_2$. A solution of KN(SiMe$_3$)$_2$ (8.7 mg, 0.044 mmol) in 0.3 mL of C_6D_6 was added to a slurry of **3a** in 0.6 mL of C_6D_6. The mixture was stirred for 1.5 h, and the color changed from orange-yellow to dark orange, with some solid precipitate present. The ^{1}H NMR spectrum showed that Cp*IrN*t*-Bu was the major product. The benzene was removed in vacuo, and the residue was extracted with pentane. The pentane was removed in vacuo; the ^{1}H NMR spectrum of the residue showed a mixture of Cp*IrN*t*-Bu (~85%) and some unidentified impurities.

Cp*Ir(DIPPNH$_2$)Cl$_2$ (3d, DIPP = 2,6-(*i*-Pr)$_2$C$_6$H$_3$). 2,6-Diisopropylaniline (0.30 mL, 1.4 mmol) was added by syringe to a solution of [Cp*IrCl$_2$]$_2$ (542 mg, 0.68 mmol) in 15 mL of CH_2Cl_2. The solution was stirred for a few min and then filtered. The filtrate was concentrated and layered with hexanes. Orange crystals were isolated by filtration and washed with hexanes to give 0.708 g of **3d** (90%): IR (KBr) 3266, 3197, 3105, 2964, 2919, 1559, 1478, 1376, 1276, 1159, 1029 cm^{-1}. Anal. Calcd for $C_{22}H_{34}IrNCl_2$: C, 45.90; H, 5.97; N, 2.43. Found: C, 45.82; H, 5.87; N, 2.37.

Cp*IrNDIPP (1d) via Cp*Ir(DIPPNH$_2$)Cl$_2$. A solution of KN(SiMe$_3$)$_2$ (0.29 g, 1.5 mmol) in 5 mL of toluene was cooled to −40 °C and added dropwise with stirring to a similarly cooled solution of **3d** (0.40 g, 0.70 mmol) in 50 mL of toluene. After stirring the orange solution for 5 h, the volatile materials were removed in vacuo. The residue was extracted with hexane. The hexane solution was concentrated to 12 mL and cooled to −40 °C to afford **1d** as orange-yellow crystals which were manually separated from darker red crystals of an unidentified impurity and washed with cold hexane. IR (KBr) 2952, 2917, 1480, 1462, 1419, 1359, 1351, 1300, 1032, 1023, 992, 796, 761, 423 cm^{-1}; EI-MS m/e 503, 501 (M$^+$). Anal. Calcd for $C_{22}H_{32}IrN$: C, 52.56; H, 6.42; N, 2.79. Found: C, 52.28; H, 6.48; N, 2.87. A more convenient synthetic method is the direct metathesis described below.

Cp*IrNDIPP via [Cp*IrCl$_2$]$_2$. The procedure for **1a** was followed by using 170 mg (0.213 mmol) of [Cp*IrCl$_2$]$_2$, 160 mg (0.874 mmol) of LiNHDIPP, and 15 mL of THF. Extraction of the yellow-brown residue with toluene and crystallization from toluene/pentane at −40 °C gave 164 mg of **1d** as orange-brown crystals (77%).

X-ray Crystal Structure Determination of 1d. Orange crystals were grown from toluene/hexane at −40 °C and mounted as described for **1a**. X-ray data were collected as for **1a**; the final cell parameters and specific data collection parameters are given in Table I.

The 1598 raw intensity data were reduced as above. There was no crystal decay. An empirical absorption correction was applied: T_{max} = 1.0, T_{min} = 0.693. Choice of the centric space group *Pnma* was confirmed by the successful refinement of the structure. Removal of systematically absent data left 1415 unique data in the final data set. The structure was solved by Patterson methods and refined via standard least-squares and Fourier techniques as for **1a** (except hydrogen atoms were not located or refined). Least-squares analysis of the data and correction for anomalous dispersion were carried out as for **1a**; the p factor was set to 0.03. The final residuals for 58 variables refined against the 1181 data for which $4F^2 > 3\sigma(F^2)$ were R = 1.9%, wR = 3.9%, and GOF = 1.93. The R value for all 1415 data was 4.4%. The largest peak in the final difference Fourier map had an electron density of 0.75 e$^-$/Å^3 and the lowest excursion −0.63 e$^-$/Å^3.

Reaction of Cp*IrN*t*-Bu with Arylamines: (1) Cp*IrNXy from Cp*IrN*t*-Bu. (a) An NMR tube was charged with a mixture of Cp*IrN*t*-Bu (**1a**) (5 mg, 1.3 × 10^{-2} mmol) and XyNH$_2$ (5 mg, 4.1 × 10^{-2} mmol) in C_6D_6. The solution was freeze–pump–thawed, and the tube was sealed under vacuum. The ^{1}H NMR spectrum after 2 h showed peaks due to **1a**, **1c**, *t*-BuNH$_2$, XyNH$_2$, and a small amount of an unidentified purple complex (Cp* δ 1.24; Xy Me δ 2.49). After 1 day, the ^{1}H NMR spectrum showed signals due to **1c**, XyNH$_2$, *t*-BuNH$_2$, and the unidentified material. After 4 days, **1c** was consumed, and the spectrum showed only peaks due to the two amines and the purple compound, which could be isolated as purple crystals from similar reaction mixtures by recrystallization from toluene at −40 °C. It slowly decomposes in benzene solution at ambient temperature and was not characterized further.

(b) An identical procedure was followed with 99 mg of **1a** (0.25 mmol) and 30 mg of XyNH$_2$ (0.25 mmol). The ^{1}H NMR spectrum after 2 h showed a mixture of **1a**, **1c**, *t*-BuNH$_2$, XyNH$_2$, and the purple material. The ratio of the three Ir compounds was ~1.3:2:0.2, suggesting that the reaction of **1c** with XyNH$_2$ is faster under these conditions than that of **1a** with XyNH$_2$.

(2) Cp*IrNDIPP from Cp*IrN-*tBu*. An NMR tube was charged with a mixture of Cp*IrN*t*-Bu (10 mg, 2.5 × 10^{-2} mmol) and DIPPNH$_2$ (4.5 mg, 2.5 × 10^{-2} mmol) in C_6D_6. The tube was capped, and the reaction was monitored by ^{1}H NMR spectroscopy, which showed slow formation of **1d** and *tert*-butylamine with a half-life of ~2 days.

Reaction of Cp*IrN*t*-Bu with MeI. To a C_6D_6 solution (~2 mL) of Cp*IrN*t*-Bu (27 mg, 6.8 × 10^{-2} mmol) in an NMR tube was added, by syringe, methyl iodide (20 mg, 0.14 mmol). The NMR tube was capped and stored in the drybox. After 2 days, orange solid had fallen out of solution. The volatile materials were removed from the tube by vacuum transfer, and the orange residue was extracted with H_2O in the air to give a clear solution. Removing the water in vacuo gave 13 mg of white powder (79%), identified as the salt Me$_3$N*t*-Bu$^+$I$^-$ by comparison of its ^{1}H NMR and IR spectra with those of an authentic sample. The red water-insoluble residue (29 mg, 74%) was shown to be [Cp*IrI$_2$]$_2$ by comparison of its ^{1}H NMR and IR spectra with the literature values.[9]

Me$_3$N*t*-Bu$^+$I$^-$. Methyl iodide (76 mg, 0.51 mmol) was added neat to a solution of LiNH*t*-Bu (20 mg, 0.25 mmol) in 5 mL of THF. After 1 h of stirring, the mixture was cloudy. A slurry of KH (10.2 mg, 0.254 mmol) in 10 mL of THF was added to give a cloudy mixture containing suspended solids. After another 1 h of stirring, a second portion of MeI (36 mg, 0.25 mmol) was added; the mixture was stirred overnight. The white solid that formed was separated by decanting the supernatant to give 30 mg of white powder (57%). It was identified as Me$_3$N*t*-Bu$^+$I$^-$ by ^{1}H NMR and IR spectroscopy: ^{1}H NMR (D_2O) δ 2.87 (9 H, N-Me), 1.31 (t, J_{N-H} = 1.7, 9 H, *t*-Bu); IR (KBr) 1477, 1451, 1416, 1385, 1179, 953, 837, 696 cm^{-1}.

Cp*Ir(CN*t*-Bu)(*t*-BuN=C=N*t*-Bu) (4). Cp*IrN*t*-Bu (61 mg, 0.15 mmol) was dissolved in 15 mL of toluene, and the solution was freeze–pump–thawed, and then, *tert*-butyl isonitrile (86 Torr in a 66-mL bulb, 0.30 mmol) was condensed into the flask. After sitting overnight, the volatile materials were removed from the orange solution in vacuo. The orange residue was recrystallized from pentane at −40 °C to give 60 mg of yellow crystals in three crops (69%): mp 185–190 °C dec; IR (KBr) 2960, 2916, 2110 (s), 2065 (s), 1707 (s), 1688 (s), 1353, 1251, 1235, 1214, 1196 cm^{-1}; MS (FAB, sulfolane), m/e 566/564 (MH$^+$, ^{193}Ir/^{191}Ir), 483/481 ((MH − CN*t*-Bu)$^+$, ^{193}Ir/^{191}Ir). Anal. Calcd for $C_{24}H_{42}IrN_3$: C, 51.02; H, 7.51; N, 7.44. Found: C, 50.88; H, 7.50; N, 7.35.

Cp*Ir(CO)(*t*-BuNCO) (5a). A solution of Cp*IrN*t*-Bu (79 mg, 0.20 mmol) in 15 mL of toluene was freeze–pump–thawed and put under 600 Torr of CO. After sitting overnight, the excess CO and the solvent were removed in vacuo from the orange-yellow solution to give orange oil. This was recrystallized from hexane at −40 °C to give 64 mg of orange crystals in three crops (71%): mp 86–91 °C dec; IR (KBr) 2976, 1956 (s), 1801 (s), 782, 695 cm^{-1}; MS (FAB, sulfolane) m/e 455/453 (M$^+$, ^{193}Ir/^{191}Ir), 428/426 [(MH − CO)$^+$, ^{193}Ir/^{191}Ir]. Anal. Calcd for $C_{16}H_{24}IrNO_2$: C, 42.27; H, 5.33; N, 3.08. Found: C, 41.98; H, 5.32; N, 3.11.

Cp*IrPPh$_3$(*t*-BuNCO) (5b). A solution of Cp*IrN*t*-Bu (79 mg, 0.20 mmol) and PPh$_3$ (55 mg, 0.21 mmol) in 15 mL of toluene was freeze–pump–thawed and put under 600 Torr of CO. After sitting overnight, the excess CO and the solvent were removed in vacuo to give a yellow oil. This was recrystallized from hexane at −40 °C to give 70 mg of orange microcrystals in three crops (53%): mp 167–169 °C dec; IR (KBr) 2961, 1751, 1653, 1457, 1254, 1094, 697 cm^{-1}. Anal. Calcd for $C_{33}H_{39}IrNOP$: C, 57.53; H, 5.72; N, 2.03. Found: C, 57.20; H, 5.70; N, 1.97.

Cp*IrN*t*-Bu(dppePt) (6). Freshly recrystallized **1a** (40 mg, 0.10 mmol) and dppePt(C_2H_4) (62 mg, 0.10 mmol) were dissolved in 30 mL

of THF. The initially yellow-orange and slightly cloudy solution was stirred for 1 h, during which time it became deeper orange. After 24 h, the solvent was removed in vacuo from the now red-orange solution. The remaining light orange powder was dissolved in 5 mL of toluene. The red solution was filtered through Celite and concentrated to ~1 mL. Addition of pentane and cooling to −40 °C gave feathery light orange crystals in several crops (69 mg, 70%): IR (KBr) 3069, 3051, 2956, 2907, 1483, 1436, 1198, 1098, 1028, 877, 813, 748, 698, 672, 527, 486 cm^{-1}. Anal. Calcd for $C_{40}H_{48}IrNPPt$: C, 49.98; H, 5.04; N, 1.46. Found: C, 49.61; H, 4.85; N, 1.28.

Cp*Ir(N*t*-BuOCO) (7a). A yellow solution of Cp*IrN*t*-Bu (52 mg, 0.13 mmol) in 15 mL of pentane was freeze–pump–thawed, refrozen, and evacuated, and CO_2 (275 Torr in a 66-mL bulb, 0.98 mmol) was condensed into the flask at liquid nitrogen temperature. Upon thawing, the solution turned red and red crystals formed. After sitting overnight, 48 mg of red crystals (83%) were collected: mp 120 °C dec; IR (C_6H_6 solution) 1708 cm^{-1}; MS (FAB, sulfolane) *m/e* 443/441 (M^+, $^{193}Ir/^{191}Ir$). Despite several attempts, analyses for carbon were low, for example, Anal. Calcd for $C_{15}H_{24}IrNO_2$: C, 40.70; H, 5.48; N, 3.17. Found: C, 39.34; H, 5.20; N, 2.90.

X-ray Crystal Structure Determination of 7a. Clear red platelike crystals were obtained from vapor diffusion of hexamethyldisiloxane into toluene at −40 °C and mounted as described for **1a**. X-ray data were collected as for **1a**; the final cell parameters and specific data collection parameters are given in Table I.

The 1266 raw intensity data were reduced as above. They were corrected for a reduction of 37% of the original intensity of measured standards. An empirical absorption correction was applied to the data (T_{max} = 1.0, T_{min} = 0.63). Inspection of the systematic absences indicated possible space groups *Pnma* and $Pn2_1/a$. The choice of *Pnma* was confirmed by the successful solution and refinement of the structure. Removal of systematically absent and averaging of redundant data left 1110 unique data in the final data set.

The structure was solved by Patterson methods and refined via standard least-squares and Fourier techniques as for **1a** (including treatment of the hydrogen atoms). Least-squares analysis of the data and correction for anomalous dispersion were carried out as for **1a**; the *p* factor was set to 0.03. The final residuals for 100 variables refined against the 911 data for which $F^2 > 3\sigma(F^2)$ were R = 1.94%, wR = 2.33%, and GOF = 1.193. The R value for all 1110 data was 3.81%. The largest peak in the final difference Fourier map had an electron density of 0.38 $e^-/Å^3$ and the lowest excursion −0.95 $e^-/Å^3$. Both were located near the Ir atom. There was no indication of secondary extinction in the high-intensity low-angle data.

Cp*IrPPh$_3$(N*t*-BuOCO) (7b). A toluene (5 mL) solution of PPh_3 (35 mg, 0.13 mmol) was added dropwise to a red solution of Cp*Ir(N*t*-BuOCO) (48 mg, 0.11 mmol) in 10 mL of toluene. The solution immediately bleached and became yellow-orange. Concentration of the solution gave 53 mg of yellow crystals (69%). This compound is exceptionally water-sensitive and reacts with traces of water on glassware to give *t*-BuNH_2 and presumably the carbonate complex Cp*IrPPh_3CO_3: mp 129–140 °C dec; IR (KBr) 1621, 1312 cm^{-1}, (CH_3CN solution) 1628, 1299 cm^{-1}; MS (FAB, sulfolane) *m/e* 706/704 (MH^+, $^{193}Ir/^{191}Ir$), 661/659 [$(M - CO_2)^+$, $^{193}Ir/^{191}Ir$]. Multiple carbon analyses for this material gave high values, for example, Anal. Calcd for $C_{33}H_{39}IrNO_2P$: C, 56.22; H, 5.59; N, 1.99. Found: C, 59.00; H, 5.96; N, 1.87.

Cp*Ir(RCCRN*t*-BuRCCR) (R = CO$_2$Me) (8). A solution of dimethylacetylenedicarboxylate (77 mg, 0.54 mmol) in 5 mL of toluene was added dropwise to a solution of Cp*IrN*t*-Bu (104 mg, 0.261 mmol) in 15 mL of toluene. After sitting overnight, the volatile materials were removed in vacuo from the orange-brown solution. The brown residue was recrystallized from toluene layered with hexane at −40 °C to give 121 mg of golden-brown crystals (68%): mp 187–192 °C dec; IR (C_6H_6 solution) 2950, 1723 (s), 1703 (shoulder), 1435, 1206, 1122 cm^{-1}; MS (FAB, sulfolane) *m/e* 684/682 (MH^+, $^{193}Ir/^{191}Ir$), 626/624 ($M - t$-Bu)$^+$, 568/566 ($MH - t$-Bu $- CO_2Me)^+$. Anal. Calcd for $C_{26}H_{36}IrNO_8$: C, 45.73; H, 5.32; N, 2.05. Found: C, 45.56; H, 5.34; N, 2.11.

X-ray Crystal Structure Determination of 8. Clear pale yellow platelike crystals were obtained from vapor diffusion of hexamethyldisiloxane into toluene at −40 °C and mounted as described for **1a**. X-ray data were collected as for **1a**; the final cell parameters and specific data collection parameters are given in Table I.

The 4013 raw intensity data were reduced as above. The data were corrected for a 2.9% decay of intensity standards. An empirical absorption correction was applied to the data (T_{max} = 1.0, T_{min} = 0.76). Inspection of the systematic absences indicated uniquely space group $P2_1/c$. Removal of systematically absent and redundant data left 3622 unique data in the final data set. The structure was solved by Patterson methods and refined via standard least-squares and Fourier techniques as for **1a** (including treatment of the hydrogen atoms). Before the final refinement, three reflections were removed from the data set due to errors.

Least-squares analysis of the data and correction for anomalous dispersion were carried out as for **1a**; the *p* factor was set to 0.03. The final residuals for 326 variables refined against the 3103 data for which $F^2 > 3\sigma(F^2)$ were R = 2.11%, wR = 2.79%, and GOF = 1.468. The R value for all 3619 data was 3.74%. In the final cycles of refinement a secondary extinction parameter was included (maximum correction—18% on F). The largest peak in the final difference Fourier map had an electron density of 0.72 $e^-/Å^3$ and the lowest excursion −1.02 $e^-/Å^3$. Both were located near the Ir atom.

Cp*Ir[N*t*-BuC(O)CH=CHCO$_2$] (9a). To a yellow solution of Cp*IrN*t*-Bu (112 mg, 0.281 mmol) in 10 mL of toluene was added dropwise a clear solution of maleic anhydride (27 mg, 0.275 mmol) in 5 mL of toluene. The solution immediately became a more intense yellow and then orange-yellow. The mixture was shaken vigorously and then set aside for 5 min, while orange-yellow microcrystals fell out of solution. The mixture was cooled to −40 °C for 5 h. The supernatant was then removed with a pipet to give 103 mg of yellow needles (74%), from which residual solvent was removed under vacuum: mp 120–125 °C dec; IR (KBr) 3006, 2969, 2925, 1698, 1642, 1321, 1246 cm^{-1}; MS (FAB, sulfolane) *m/e* 497/495 (M^+), 453/451 $(M - CO_2)^+$. Anal. Calcd for $C_{18}H_{26}IrNO_3$: C, 43.53; H, 5.29; N, 2.82. Found: C, 43.15; H, 5.21; N, 2.71.

Cp*Ir[N*t*-BuC(O)CH=CHCO$_2$](CO) (9b). A solution of freshly prepared **9a** (100 mg, 0.311 mmol) in 15 mL of acetone in a glass bomb was freeze–pump–thawed, frozen, evacuated, and placed under 700 Torr of CO. The bomb was sealed and heated to 45 °C for 15 h. The excess CO and the solvent were removed from the orange solution in vacuo to give an orange oil. This was recrystallized from toluene at −40 °C to give 65 mg of very pale yellow microcrystals in two crops (61%): mp 155 °C dec; IR (KBr) 3014, 2964, 2917, 1994, 1602, 1560, 1341, 1192 cm^{-1}; MS (FAB, sulfolane) *m/e* 482/480 [$(MH - CO_2)^+$, $^{193}Ir/^{191}Ir$], 454/452 [$MH - CO_2 - CO)^+$, $^{193}Ir/^{191}Ir$]. Anal. Calcd for $C_{19}H_{26}IrNO_4$: C, 43.49; H, 5.01; N, 2.67. Found: C, 43.73; H, 5.40; N, 2.80.

Acknowledgment. We are grateful for support of this work from the National Institutes of Health (Grant No. GM-25459). We also thank Professor R. A. Andersen for helpful discussions and Mr. Richard I. Michelman for preparing a sample of labeled Cp*Ir^{15}NtBu and obtaining its ^{15}N NMR spectrum. We acknowledge the Johnson-Matthey Co. for a loan of $IrCl_3 \cdot 3H_2O$, and Jim Gilchrist and Professor David Collum (Cornell University) for details of their *t*-Bu$^{15}NH_3Cl$ synthesis. We thank Professor Paul Sharp for encouraging us to include a discussion of the bonding of Cp*IrNR complexes in the paper.

Supplementary Material Available: Tables of positional and thermal parameters for **1b–d** and **8** (6 pages). Ordering information is given on any current masthead page.